A General Observational Strategy for Validation of Satellite NO2 Retrievals using Multi-Axis Differential Optical Absorption Spectroscopy (MAX-DOAS)

Jeffrey D Earley

Thesis submitted to the Faculty of the

Virginia Polytechnic Institute and State University

in partial fulfillment of the requirements for the degree of

Masters of Science

in

Electrical Engineering

Elena S. Lind, Chair

Yizheng Zhu

Hosein Foroutan

May 10, 2022

Blacksburg, Virginia

Keywords: MAX-DOAS, Validation, Ground Sampling

A General Observational Strategy for Validation of Satellite NO2 Retrievals using Multi-Axis Differential Optical Absorption Spectroscopy (MAX-DOAS)

Jeffrey D Earley

(ABSTRACT)

This thesis analyzes the effectiveness of spatially averaged Multi-AXis Differential Optical Absorption Spectroscopy (MAX-DOAS) measurements at regular azimuth angle intervals on an hourly basis to validate satellite based DOAS measurements. Off-Axis MAX-DOAS Measurements taken in Blacksburg, Virginia, between November 2021 and April 2022 with an evenly distributed set of measurements were averaged every hour and compared to Direct Sun measurements, also averaged every hour. Comparisons of the difference in average measurement from both measuring strategies, as well as the distribution standard deviations of hourly measurements suggests that the NO_2 distribution around Blacksburg is homogeneous. In order to test the effectiveness of this sampling strategy,in an inhomogeneous location, the LOTOS-EUROS high resolution (1kmx1km) chemical transport model was used to simulate profiles and vertical column densities of real measurements taken during the TROLIX'19 Field Campaign. The LOTOs-EUROS model was used to simulate vertical profiles as well as Vertical Column Densities based on real MAX-DOAS measurements as well as TROPOMI viewing geometry. While the individual ground measurements were not equal to the TROPOMI profile, the TROPOMI profile is approximately the average of the profiles of measurements made within the hour of TROPOMI overpass.

A General Observational Strategy for Validation of Satellite NO2 Retrievals using Multi-Axis Differential Optical Absorption Spectroscopy (MAX-DOAS)

Jeffrey D Earley

(GENERAL AUDIENCE ABSTRACT)

This thesis analyzes the effectiveness of spatially averaged Multi-AXis Differential Optical Absorption Spectroscopy (MAX-DOAS) measurements at regular intervals of angles offset from due North on an hourly basis to validate satellite based DOAS measurements. MAX-DOAS Measurements taken relative to the position of the sun in Blacksburg, Virginia, a low NO_2 location, between November 2021 and April 2022 to determine the effectiveness of a generalized measuring strategy for satellite validation in low pollution environments. An evenly distributed set of measurements were averaged every hour and compared to measurements taken in the direction of the sun, also averaged every hour, to determine if the variability of NO_2 around Blacksburg is high enough to require a generalized sampling strategy, or if the NO_2 distribution is homogeneous enough to be accurately validated with Direct Sun measurements only.. Comparisons of the difference in average measurement from both measuring strategies, as well as the distribution of standard deviations of hourly measurements suggests that the NO_2 distribution around Blacksburg is low. In order to test the effectiveness of this sampling strategy in a higher pollution location with many sources and sinks of NO_2, the data from the LOTOS-EUROS high resolution (1kmx1km) chemical transport model run by the Royal Dutch Meteorological Institute for the TROLIX'19 Field Campaign was used to simulate vertical distributions of NO_2 and vertical column densities of measurements taken during the field campaign. The LOTOS-EUROS model was used to simulate vertical distributions of NO_2 as well as Vertical Column Densities based on real MAX-DOAS measurements as well as viewing geometry seen by the TROPOspheric Monitoring Instrument

(TROPOMI) satellite-based instrument. While the individual ground measurements were not equal to the vertical distribution seen by TROPOMI, the TROPOMI vertical distribution is approximately the average of the vertical distributions of measurements made within an hour of TROPOMI passing over Rotterdam.

Contents

Chapter 1

Thesis objectives and Organization

1.1 Thesis goals and objectives

The goal of this thesis is to determine the viability of spatially sampling measurements to improve satellite validation in environments with homogeneous and inhomogeneous distributions of NO_2. Therefore, at a measuring site with a homogeneous distribution of NO_2, Blacksburg, Virginia, two measuring strategies, one that measures a large air volume and one that measures a smaller air volume, are measured simultaneously and comparisons between the two strategies made can be used to determine the effectiveness of the sampling strategy in a homogeneous environment. The effectiveness of the two sampling strategies can be used to determine whether or not a large volume of air must be sampled in order to properly validate satellite-based measurements, or if a small volume of air can adequately represent the spatial variability of measurements for locations similar to Blacksburg. For ground-based validation in an inhomogeneous environment, simulated vertical distributions of NO_2 based on real measurements can be used to show the effect that viewing direction has on the profiles retrieved as well as in comparison to profiles seen by satellite-based in-

struments. These vertical distributions will show the effect of horizontal inhomogeneity on individual measurements when compared to satellite measurements, and show a possible cause of the differences in retrievals between satellite and ground-based measurements.

1.2 Thesis organization

This thesis is as organized as follows: Chapter 1 describes the basic outline and objectives of this thesis. Chapter 2 introduces the NO_x family of trace gases, with an emphasis on NO_2, by explaining its impact on human health, as well as its distribution in the atmosphere. Next Differential Optical Absorption Spectroscopy, a remote sensing method that is commonly used to determine NO_2 pollution quantities and is used in this thesis, is described as well as the relevant satellite based instruments and current ground based validation strategies using Multi-Axis Differential Optical Absorption Spectroscopy. One major issue in ground-based satellite validation is the underestimation of pollution quantities retrieved from satellite measurements when compared to ground-based measurements. In order to characterize this discrepancy, Chapter 3 proposes a possible measuring strategy to improve satellite validation, as well as comparisons made to a different strategy that measures a smaller volume of air than the proposed strategy. In addition, the methodology used to simulate vertical distributions of NO_2 is explained. Chapter 4 shows the results of the data collected and analyzed according to Chapter 3. Chapter 5 makes conclusions based on the results shown in Chapter 4. Finally, Chapter 6 gives further work that can be done on this topic to further understand the impact that measuring strategies have on satellite validation.

Chapter 2

Introduction

2.1 Ground-based remote sensing of NO_2

2.1.1 Nitrogen Oxides

Nitrogen Oxides ($NO_x = NO_2 + NO$) are trace gasses that play an important role in both stratospheric and tropospheric chemistry, being responsible for ozone and aerosol production in both atmospheric layers. While there are many biogenic sources of NO_x, such as soil chemestry and lightning, the primary sources are anthropogenic; pollution from combustion engines and power generation are the primary sources for NO_x [33] [17]; as such NO_2 pollution distributions tend to be centered around urban centers, where vehicle density is at its largest [34]. Not only does NO_x drive tropospheric Ozone formation and stratospheric Ozone Depletion, exposure to NO_2 can lead to adverse health effects, such as Pulmonary Inflammation [17], susceptibility to respiratory infection [17] decreases in lung function and an increase in susceptibility to allergens for people with asthma [44] [39]. Anthropogenic NO_2 has a relatively short lifetime at approximately 3.8 hours [36]; this means that NO_2

pollution remains close to its source, and can be used to track pollution sources.

Vertical Profiles of Nitrogen Dioxide are heavily influenced by the Planetary Boundary Layer (PBL). The PBL is the lowest layer of the troposphere, which is connected to the planet's surface. Because of this, the PBL is the primary location of anthropogenic emissions and is where the majority of tropospheric chemistry occurs. Zhang et al. [50] determined that the height of the PBL during the day is proportional to air temperature, and inversely proportional to relative humidity by comparing daily radiosonde measurements taken at 12:00 Local Time at 26 locations around Europe over a period of 30 years. Average yearly heights for the PBL around Europe range between 0.5km and 1.5km. Due to the shorter lifetime of NO_2 when compared to transport from the surface to the free troposphere, which is approximately one week, NO_2 profiles remain below the PBL. Wang et al. [49] demonstrates this concept by developing profiles of many trace gases, including NO_2, in Northern China . Maximum concentrations of NO_2 were found in the morning, due to both an increase in vehicular emissions in the morning as well as the combination of higher relative humidity and lower temperatures in the morning decreasing the height of the PBL. The average profile height for NO_2 is estimated to be approximately 1.2km, with a minimum on high pollution mornings at 0.5km.

In order to quantify NO_2 exposure, there are a number of different methods that can be used. In-Situ methods measure NO_2 concentrations at the measuring location only. These measurements are only valid for areas on the microscopic scale, and represent the concentrations seen at an exact location. Remote sensing methods, on the other hand, measure concentrations in a given volume of air. The of this volume can change depending on the type of viewing geometry and measuring technique used. For instance, due to the large distance between a satellite's orbit and the Earth's surface, satellite-based measurements will measure a large volume of air, approximately a column with a cross sectional area on kilo-

meter scales, through the entirety of the atmosphere. Ground-based measurements instead measure a smaller volume of air, which can be approximated as a cone with radii in the hundreds of meters range and distances between 10-20km. One remote sensing technique that is commonly used for retrievals of NO_2 air quality data is differential optical absorption spectroscopy, which is also used to retrieve NO_2 data in this thesis.

2.1.2 Differential Optical Absorption Spectroscopy

Differential Optical Absorption Spectroscopy, (DOAS) is a spectroscopic technique used to retrieve information on trace gas concentrations from light spectra [31]. Like other remote sensing techniques, the DOAS techniques begins with the measuring of solar radiance or irradiance, depending on if the light measured is unscattered or scattered, respectively. The measurements are performed in one of three viewing geometries: Direct Sun, which measures unscattered sunlight, Multi-Axis DOAS, which measured scattered light in distinct azimuth and zenith directions in the sky, and Zenith Scattered light, not used in this thesis, which measures scattered sunlight that has been scattered into the light path of the instrument directly overhead the measuring site. Next the measured spectra are corrected for instrumental errors such as: Dark current, spectrometer non-linearity, pixel response nonuniformity, spectrometer temperature sensitivity, wavelength shifting, stray light, etc [6]. After this, absorption cross section is fitted to the differential optical depth, which is the natural log of the ratio between the reference and measured intensities, to retrieve the differential slant column density of the measurement, the difference between slant column densities of the measurement and reference measurement. Finally, the differential slant column densities can be converted to their final data products. In the case of the Direct Sun geometry, dSCD's can be converted to vertical column densiteis through the use of the air mass factor. For MAX-DOAS measurements, measurements made in a given set of measured zenith an-

gles can be converted to vertical profiles through the use of inverse modelling with radiative transfer models.

Like classical optical absorption spectroscopy, DOAS is derived from the Beer-Lambert Law, which states that a measured light intensity (I) is equal to the original reference intensity (I_0) multiplied by the exponential of the wavelength absorption cross section ($\sigma(\lambda)$) multiplied by the gas concentration (c) and the path length (L), or:

$$I = I_0 e^{-\sigma(\lambda)*c*L}. \tag{2.1}$$

However, this equation is for only one trace gas being measured. For more complex gas mixtures, the exponential becomes a summation of all trace gas concentrations in the mixture multiplied by each absorption cross section and the common path length, in addition to Rayleigh and Mie scattering effects. This method becomes exceedingly complicated for any measurements made outside of a lab setting; Air is a good example of this, since air is composed mainly of N_2 and O_2 there are already two major absorbers that have to be taken into account before any trace gasses can be considered, and since normally each trace gas will be retrieved individually, this means that there are a lot of cross sections and concentrations to deal with, before even taking into account non-absorbing effects, such as Rayleigh and Mie scattering. DOAS overcomes this complexity by taking advantage of the fact that absorption cross-sections can be separated into two parts, with σ_0 representing the broadband structures of the cross-section with slow variations in λ, and σ‘, representing the narrowband structures of he cross-section that vary rapidly with λ. Now, the Beer-Lambert law becomes, after also adding in scattering effects such as Rayleigh and Mie scattering:

$$I = I_0 e^{-L\Sigma\sigma'(\lambda)_j c_j}(b_0 + b_1 x + b_2 x^2) \tag{2.2}$$

The differential absorption cross section, $\sigma'(\lambda)$, of each trace gas of interest is determined through laboratory testing using high resolution instrumentation to accurately measure the high frequency structure of the absorption cross section. These high resolution absorption cross sections can been be convoluted with the instrumental slit function to match the resolution of the instrument to be used in DOAS retrievals. Now that these two terms are separated, the intensity in the absence of differential absorption can estimated as a polynomial ($b_0 + b_1 x + b_2 x^2$), and represents the fitted approximation of wideband structures in the absorption cross section, as well as scattering effects. After substituting the differential cross section into the Beer-Lambert equation, the differential optical density can be calculated using the ratio between a measured intensity and a reference intensity, and the following conclusion can be reached:

$$D' = ln(\frac{I'_0(\lambda)}{I(\lambda)}) = \Sigma \sigma'_j L_j c_j \tag{2.3}$$

where D' is the differential optical density of a layer for j different absorbers. The absorption cross section of each trace gas is unique, therefore careful selection of wavelength intervals to analyze will allow trace gases to be retrieved individually. The differential optical depth can be used to determine the slant column density (SCD) of the measurement, which corresponds to the amount of trace gas concentration integrated along the light path. These slant column densities can be converted to vertical profiles as well as vertical column densities through the use of radiative transfer modelling and weighting functions [12], which describe the sensitivity of intensity to gas perturbations at each atmospheric layer of the model.

The Ring Effect, originlally identified by Grainger and Ring [15] in 1962, describes the difference in shape of Fraunhofer Solar absorption lines when measuring direct and scattered sunlight. The cause of this phenomena has been identified as rotational Raman Scattering [3] and can affect optical density by a maximum of a few percent, which significantly affects DOAS retrievals [18]. To account for this effect, a Fraunhofer Reference Spectrum can be

used during DOAS retrievals of scattered sunlight by fitting for a pseudo-absorber to detect light path enhancements due to the increased complexities of ratiative transfer when dealing with scattered light [18].

2.1.3 Direct sun DOAS

Direct Sun Differential Optical Absorption Spectroscopy measures unscattered solar radiance for DOAS retirevals. Figure 2.1 shows a diagram of a typical direct sun measurement. Since the vast majority of light collected is unscattered, this means the path length of each retrieval will be much longer than scattered light methods, allowing for sensitivity to both stratospheric as well as tropospheric profiles. The path length observed changes as a function of solar position, as the sun tracks overhead, the path length decreases until it is at its minimum at zenith.

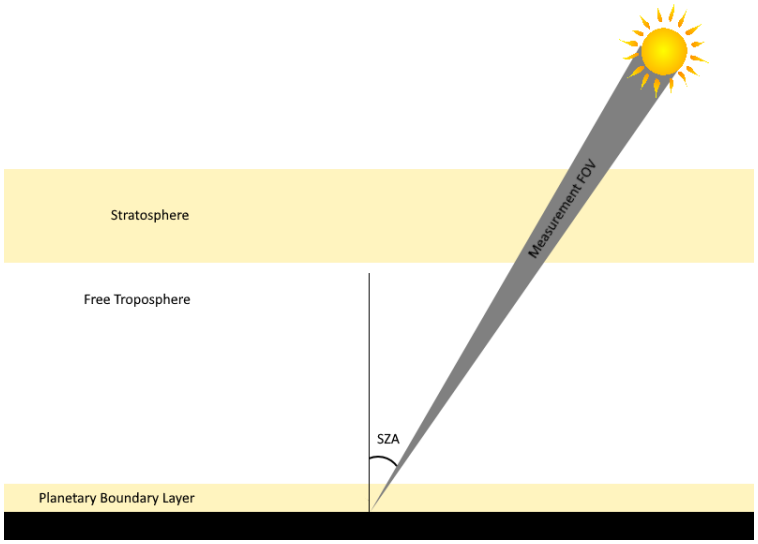

Figure 2.1: Diagram of a Direct Sun DOAS Measurement [31]

This sensitivity can be described by the solar zenith angle (SZA) which is 0° when directly overhead, and 90° at the horizon. In order to quantify direct sun measurements, the slant

column density is normally used, and is defined as the concentration of trace gas integrated over the path length within the entire atmosphere.

$$S = \int_0^\infty c(s)ds \tag{2.4}$$

where ds is in the direction of the sun. This column density is only an apparent one, however, which is highly difficult to interpret due to the myriad of possible path lengths each measurement observes. Therefore, it is easier to describe the slant column density by the differential optical depth D' and the differential absorption cross section σ': $S = \frac{D'}{\sigma'}$. In order to relate the SCD to a more useful quantifier, the Vertical Column Density, the ratio between the two densities, the air mass factor, can be used. The AMF can also be related to the slant length, L, and the vertical path length, Z, and can be estimated based on the solar zenith angle:

$$AMF = \frac{L}{Z} = sec\left(sin^{-1}\left(\frac{R}{R + h_{eff}} \cdot sin(SZA^*)\right)\right) \tag{2.5}$$

Where R is the radius of the Earth from the center to the measuring site, h_{eff} is the effective height of the trace gas profile to be retrieved, and SZA* is the solar zenith angle corrected for atmospheric refraction. This AMF equation addresses the sensitivity to the tropospheric profile at solar zenith angles above 75°, which allows the total column density measured by the direct sun method to be accurately at solar zenith angles below with negligible change in measurement accuracy 80° [41].

2.1.4 Multi-axis DOAS

Multi Axis Differential Optical Absorption Spectroscopy (MAX-DOAS) [18] [31] is a DOAS measuring technique that uses scattered sunlight from various azimuth and zenith angles to retrieve slant column densities of trace gases. The absorption of trace gases as determined by ground based measurements depend predominantly on the distribution of light paths through the atmosphere; these light paths are influenced by aerosols in the boundary layer, which determine the last scattering altitude of the measured irradiance. Since scattered light can travel along any number of light paths, atmospheric radiative transfer must be properly described. Retrievals of Vertical Column Densities, the data product most commonly retrieved from DOAS measurements, as well as vertical profiles of trace gas concentrations can be made through the use of inverse modelling and optimal estimation of atmospheric radiative transfer conditions [12] [43] [21] which uses a priori trace gas profiles to fit a model of atmospheric conditions and sensitivities to gas perturbations in the atmosphere, the weighting functions fitted can then be used to retrieve profiles based on the differential slant column densities retrieved. However, mathematically the MAX-DOAS technique can be best understood by assuming the light detected has been scattered a single time at an identical point in space, rather than attempting to model the path lengths of individual photons that are affected by multiple scattering events that occur for scattered; this is called the single scattering approximation. The approximate path length that is assumed by the single scattering approximation can be estimated by using the effective length of O_2O_2 collisional complex retrievals [11]. The O_4 profile is directly proportional to the profile of air, which itself can be measured through meteorological measurements of air pressure and temperature, and dSCD's of O_4 can be retrieved through the DOAS technique. The ratio between the dSCD of O_4 and the profile of O_4.

$$L \approx \frac{dSCD_{O_4}}{c_{O_4}} \tag{2.6}$$

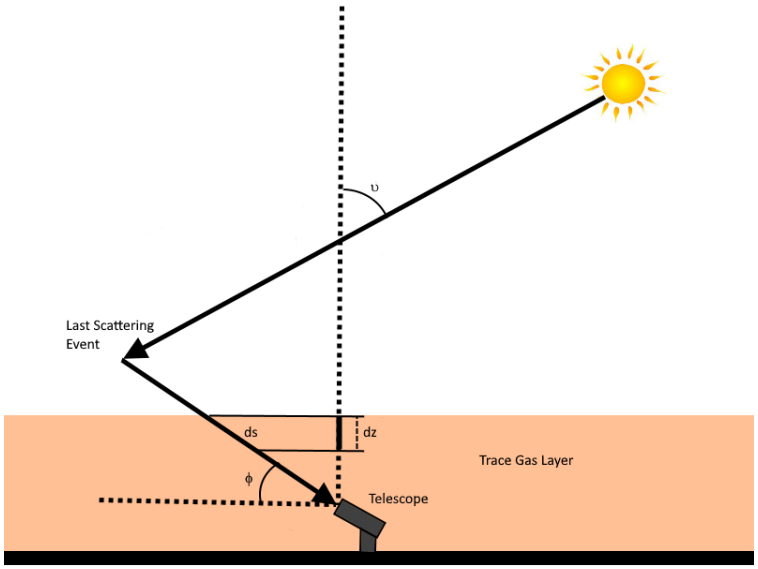

Figure 2.2: Diagram of a MAX-DOAS Measurement

The slant column density retrieved through MAX-DOAS is defined as the trace gas concentration derived along the effective light path, which is the average of an infinite number of different light paths:

$$S = \int_0^L c(s)ds = \frac{D}{\sigma'} \tag{2.7}$$

However, the slant column density requires knowledge of the intensity of light at the top of the atmosphere, which is unknown to ground-based measurements. Therefore, the differential slant column density (dSCD) can be retrieved instead, which is the measured intensity at a

given reference angle; for MAX-DOAS, the reference angle is vertical, at a 90° zenith angle.

$$\Delta S = \frac{D'}{\sigma'} = \frac{ln(\frac{I(90°)}{I(\phi)})}{\sigma'}) = S(\phi) - S(90°) \tag{2.8}$$

where ϕ is the zenith angle of the measurement. The information that can be gained from the dSCD, however, is only the difference in slant column densities measured, and does not give information about the absolute trace gas concentrations around the measuring site.The vertical column density, on the other hand, is defined as the vertical trace gas concentration integrated along a vertical light path:

$$V = \int_0^\infty c(z)dz \tag{2.9}$$

The VCD is a more convenient data product than either slant column density because it represents the total concentration of a trace gas above a measuring site, and is neither relative to another measurement nor measured along an unknown light path, its path is the length of the atmosphere, or in the case of tropospheric vertical column densities, the height of the troposphere. In addition, the Air Mass Factor (AMF) is the ratio between the SCD and VCD retrieved by a single measurement, and the differential air mass factor, dAMF, is the ratio between the dSCD and VCD retrieved by a single measurement:

$$A(\lambda, \upsilon, \alpha, \phi) = \frac{S(\lambda, \upsilon, \alpha, \phi)}{V} = \frac{a}{sin(\phi)} + \frac{(1-a)}{cos(\upsilon)} \tag{2.10}$$

$$\Delta A = \frac{dSCD}{V} \tag{2.11}$$

where λ is the wavelength of light, υ is the solar zenith angle, a is the fraction of the vertical trace gas column below the scattering altitude, and α and ϕ are the measurement azimuth and zenith angles, respectively. This means that the AMF is sensitive mainly to these four

quantities. Firstly, AMF is sensitive to the wavelength of light collected. This sensitivity comes from scattering effects; larger wavelength sensitivity comes from Mie scattering while smaller wavelength sensitivity is due to Rayleigh scattering . AMF is also sensitive to the measurement zenith angle. As the instrument observes scattered light at higher angles, the concentrations observed will change as well. For instance, at low elevation angles, the observations will be predominantly of tropospheric trace gases, below the boundary layer. By contrast, higher elevation angles will observe trace gases at higher elevations in the atmosphere; this is most evident in zenith-sky DOAS, which is most sensitive when measuring stratospheric trace gases [47]. The AMF sensitivity to SZA can largely be summarized by its effect on the first and last scattering altitudes. The FSA is strongly dependent on the SZA, exhibiting an exponential growth as the SZA approaches 90°. In contrast, the LSA is not dependent on the SZA. This means that as long as the FSA is above the absorbing layer, the AMF becomes largely independent of the SZA, as is the case for tropospheric absorbers. Finally, for horizontally inhomomogenous trace gas distributions, the azimuth viewing angle of the AMF becomes important. In urban areas, this inhomogenity arises due to an unequal distribution of trace gas emissions below the boundary layer. This is not the case for rural areas, where most trace gases are transported from more urban areas, however inhomogenities can still arise due to the distribution and effectiveness of chemical transport mechanisms.

In addition, the shape and altitude of the trace gas profile can affect sensitivity. For instance, Wang et al. [49] and Li et al. [23] demonstrated that measurements made in a single azimuth direction over a zenith scan with at least seven zenith angles can be used to determine the vertical profile of trace gas above the measuring site. For trace gases that reside close to the surface of the Earth, all but the smallest measuring zenith angles will have the profile below their scattering altitude, which are the profiles of interest for MAX-DOAS. This causes the

AMF approximation to only be a function of the measuring zenith angles, and is considered the tropospheric component of a trace gas column. Conversely, the stratospheric component of the trace gas column, which resides above the scattering altitude, is sensitive to the solar zenith angle only. In practice, trace gas vertical columns will have relevant components both above the scattering altitude and below it, however using the AMF approximation above is a good way to separate the two components so that they may be analyzed separately.

In the context of satellite validation, MAX-DOAS retrievals can be useful for quantifying the errors in measurements made by satellite-based instruments. However, rather than relying on a single instrument at a single location taking measurements, it is more effective to validate satellites using a ground based network of instruments. These networks have the advantage of providing time coincident measurements using identical instrumentation at multiple locations, so that the only variable present in measurements is the trace gas profile of interest. These networks allow for improved satellite validation in a timely process for a wide range of atmospheric conditions.

2.1.5 Network for the Detection of Atmospheric Composition Change

Beginning with the ERS-2 GOME satellite launched in the mid 1990s, there has been a concerted effort to develop ground based remote sensing validation techniques. At measuring sites with sufficiently low tropospheric NO_2 concentrations the UV-VIS Zenith Scattered Light Differential Optical Absorption Spectroscopy (ZSL-DOAS) technique at twilight has been useful for validation of stratospheric NO_2 from Lambert et al., 1997 to present [47]. ZSL-DOAS offers increased sensitivity to NO_2 and lower sensitivity to clouds over the portion of the light path that passes through the stratosphere, while having less sensitivity to tropospheric concentrations; this allows for improved stratospheric validation over other DOAS

techniques. Multi Axis Differential Optical Absorption Spectroscopy, or MAX-DOAS [18] on the other hand is more sensitive to trace gas concentrations that lie below the last scattering altitude, which for most zenith viewing angles will be almost entirely in the troposphere.

The Network for the Detection of Atmospheric Composition Change (NDACC) is a network of over 70 ground based research stations and over 160 active instruments [8] established in 1991 with the express purpose to:

- establish long-term databases for detecting changes and trends in atmospheric composition and to understand their impacts on the mesosphere, stratosphere, and troposphere
- establish scientific links and feedbacks between changes in atmospheric composition, climate, and air quality
- to validate atmospheric measurements from other platforms (i.e. satellites, aircraft, and ground-based platforms)
- provide critical data sets to help fill gaps in satellite observations
- provide collaborative support to scientific field campaigns and to other chemistry and climate-observing networks
- and provide validation and development support for atmospheric models

The NDACC utilizes UV/Vis spectrometers that retrieve trace gas concentration using the direct sun, zenith scattered light, and MAX-DOAS measurements, however these are not the only type of instruments in the network. The Brewer-Dobson spectrometer is a UV sensing instrument, that is able to retrieve total ozone columns above each station, and has been used for validation of satellite-based Ozone retrievals [24]. They are one of the first ground based remote sensing techniques, being developed in 1957 as stratospheric ozone became a

topic of interest for atmospheric chemists. The network also uses Fourier Transform Infrared (FTIR) spectrometers that record high resolution, mid infrared solar spectra. These spectra are then analyzed using the method of optimal estimation to measure the concentration of various trace gases with vibrational-rotational modes in the mid infrared band, such as $O_3, HCl, HF, ClONO_2, HNO_3, N_2O, CH_4, CO, C_2H_6$, and HCN.

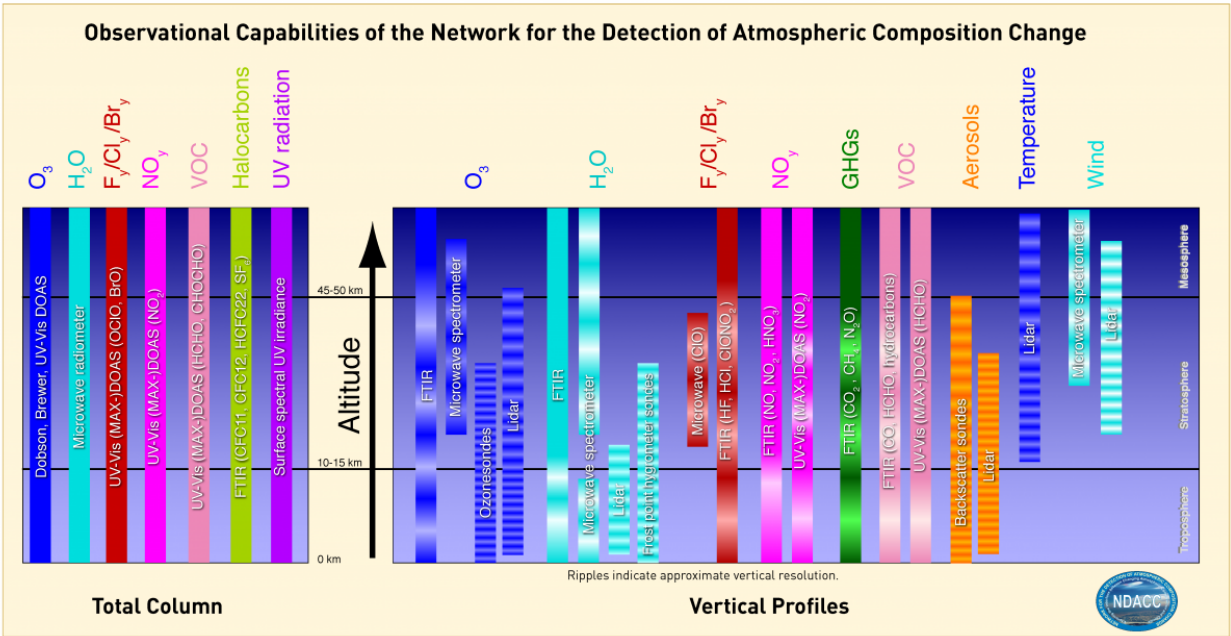

Figure 2.3: . NDACC measurement capabilities, including species and parameters measured, instrumental measurement techniques, and each measurement's approximate vertical resolution (indicated by the ripple) effect on each bar [8]

Light Detection And Ranging (LIDAR) is a laser based active remote sensing technique also used by the NDACC. LIDAR uses laser light in very discrete bands from UV to IR wavelengths, and is able to measure ozone, temperature, aerosols, water vapor, and polar stratospheric clouds at ranges from 0-10km to 30-80km, depending on the wavelengths used. Microwave spectrometers provide vertical profiles of ozone, water vapor, and ClO from the upper stratosphere and mesosphere. Retrieval is derived from the change in pressure broadening of the rotational absorption lines as a function of altitude, and can provide data on

timescales ranging from diurnal to multi-decadal.

2.1.6 Pandonia Global Network

Figure 2.4: Pandora 168 installed on the roof of Whittemore Hall, Blacksburg, Va

The Pandonia Global Network is a NASA and ESA funded network of quasi-autonomous ground stations that provide real time, standardized, calibrated, and verified air quality data to be used to verify satellite measurements [47]. This is achieved trough analyzing data from portions of the network over long time series, which overcomes issues due the the difference in field of view between satellite platforms and ground stations.

The Pandora instrument is a Passive DOAS system, which uses the sun as a light source. As sen in Figure 2.4 the head sensor collects the sunlight to be measured, with a field of view of 1.6°. The head sensor has two sets of filter wheels that can cycle between different Neutral Density filters, cutoff and cuton filters, a diffuser which is able to increase the field of view to 2.1°, and opaque and open filters. The pointing direction of the head sensor is controlled by a tracker, which the head sensor is attached to. The tracker is a set of two actuators that allows pointing in a 360° azimuth viewing range and a ±90° zenith viewing range with a pointing accuracy of 0.2°. The head sensor is connected to the spectrometer by way of a 400μm optical fiber cable; the spectrometer itself is a temperature controlled Avantes spectrometer with a dynamic range between 280 and 525nm and a spectral resolution of 0.6nm full width at half maximum. The spectrometer and the computer which records data are both inside a secure, weatherprooof case. While the instrument is quasi-autonomous, the computer is connected to the internet, allowing for remote access for monitoring, data collection, and diagnostics. Pandora instruments measure in both direct sun and scattered light multi-axis DOAS viewing geometries. A single measurement cycle is taken with an integration time between 2.4ms and 4 seconds, with repetitions made in order to improve the signal to noise ratio such that the total measurement takes approximately 40 seconds for both direct sun and MAX-DOAS measurements.

2.2 Satellite observations of NO_2

Satellite retrieval of NO_2 relies heavily on the Differential Optical Absorption Spectroscopy (DOAS) principle [26]. The individual instruments will collect spectra backscattered from the surface of the Earth. DOAS fitting of this data can then be performed for NO_2 with a fitting window between 405 and 465nm to retrieve total slant column densities within each

instrument pixel's Field of View (FOV). Next, the portion of the slant column density that lies in the stratosphere is separated from its tropospheric counterpart. The two components are very different in terms of atmospheric chemistry and therefore it is convenient to have the two separated so that both data sets can be analyzed individually. Stratospheric NO_2 can be estimated by retrieving NO_2 in remote locations, such as the Pacific Ocean where there should be almost no sources of tropospheric NO_2, over long timescales, about a month, to develop a latitudinal model of stratospheric NO_2. For tropospheric analysis, the tropospheric portion of the slant column densities (SCD) are converted to vertical column densities (VCD's). The VCD is a more quantitatively desirable value, which represents the total amount of tropospheric NO_2 above a particular location as opposed to the total column of NO_2 measured along an arbitrary path length from the satellite to the ground. This is done by dividing the tropospheric SCD by the air mass factor (AMF). The air mass factor is the ratio between the slant column density already measured and the vertical column density that is desired, and can be derived analytically. The tropospheric VCD's can then be compared to ground retrieved VCD's for validation, as well as for further air quality analysis.

2.2.1 GOME

The Global Ozone Monitoring Experiment (GOME) is a series of satellite based instruments first launched on the European Space Agency's ERS-2 satellite on 20 April 1995 (GOME-1) [16]. GOME-1 scanned a 960km swath divided over three scans, allowing for global coverage every three days; the GOME-1 pixel resolution was 320km across track and 40km along track. The GOME-1 instrument was a four channel double monochromator with a spectral range of 280-790nm and a spectral resolution of 0.2-0.4nm. While Ozone was the main target of GOME-1, retrieval of other trace gases such as $NO_2, BrO, OClO, SO_2, HCHO$, and water vapor using the DOAS technique; more specifically, NO_2 retrievals were performed with a

fitting window of 405-465nm

GOME-2 is an optical spectrometer with a dynamic range of 240–790nm and 0.26–0.51nm full width at half maximum resolution [28]. The GOME-2 swath covers a width of 1920km with a pixel resolution of 80x20km. NO_2 retrieval is performed in the same manner as GOME-1, with a fitting window of 405-465nm. GOME-2 instrument is onboard two separate satellites, Metop-A (GOME-2A) which launced on October 19, 2006, and Metop-B (GOME-2B) which launched on on April 24, 2013; both satellites continue to be operated in tandem.

It has been shown that taking Zenith Scattered Light DOAS retrievals at morning twilight in remote, low pollution locales is an effective method for GOME-1 Validation [20]. Drosoglou et al. [10] validated both GOME-2A and OMI NO_2 columns in the Thessaloniki Area, Greece, with a fitting window of 400-450nm used for ground based Validation using the DOAS technique. Pinardi et al. [29] used a similar approach, with a matching NO_2 fitting window of 405-465nm, to validate GOME-2A tropospheric columns on a global scale using instruments from the Pandonia Global Network to incorporate data from ground stations across the world. In addition,

2.2.2 SCIAMACHY

The SCanning Imaging Absorption spectroMeter for Atmospheric CartograpHY (SCIAMACHY) is a satellite borne spectrometer launched onboard the ENVISAT satellite on March 1, 2002. SCIAMACHY has a wide spectral band, 240–2380nm with 0.2–1.5nm resolution, with DOAS retrievals able to be performed in the UV/VIS portions of SCIAMACHY's measurable wavelengths [30]. SCIAMACY is able to perform observations at three different viewing geometries: nadir, limb, and solar/lunar occultation [2]. At nadir, measurments cover a swath of 30x960(across track)km with a resolution of 30x15km. Limb scans are

able to cover 960km azimuthally, and up to 150km vertically with 30x3km resolution. Solar occultation measurements have an elevation coverage of up to 150km at 2.5km resolution, at 30km along track. Retrievals of trace gasses in the UV/VIS spectral band include: $O_3, NO_2, OClO, BrO, OClO, SO_2, H_2CO$.

2.2.3 OMI

The Ozone Monitoring Instrument (OMI) is a satellite borne instrument launched by the European Space Agency in July, 2004. OMI is a nadir viewing UV/VIS (270 to 500nm) spectrometer with a spectral resolution of 0.5nm measuring backscatter radiance from the Earth's surface [22]. Its angular viewing angle is 114° which corresponds to a 2600km swath on the surface of the Earth, and has a pixel size of $13 \times 24 km^2$ at nadir, where the 13km is across track. Backscattered light entering the instrument is first depolarized then split into two different detectors, a UV detector which collects light in the 270-380nm range, and a VIS detector which collects light in the 350-500nm range. OMI utilizes 2D detectors, with one dimension of the spectrometers collecting spectral information, and the other dimension collecting horizontal data. Vertical data is collected as the instrument orbited Earth, in a push broom format.

Despite the molecule ozone in the name, OMI also retrieves other trace gas column densities, such as NO_2. Retrieval of NO_2 involves using the DOAS principle, with a fitting window between 400-450nm [10] [45]. Ground validation of OMI products are heavily dependent on well established ground remote sesning networks, such as the AERONET for retrieval of aerosol optical depths, the Brewer–Dobson network for retrieval of ozone total columns, and the Pandonia Global Network for retrieval of trace gas columns. For instance, Pinardi et al. [29] validated OMI NO_2 columns, in addition to GOME-2A columns, with a 405-465nm

fitting window, with instruments from the Pandonia Global Network.

2.2.4 TROPOMI

The Tropospheric Monitoring Instrument (TROPOMI) was launched onboard the European Space Agency's Copernicus Sentinel 5 Precursor (S5P) satellite on October 13, 2017 [14]. The S5P follows a sun-synchronous low Earth orbit at an altitude of 825km with an equatorial overpass time of 13:30 local time and period of 100 minutes which allows for daily global coverage. The TROPOMI sensor itself is a passive optical satellite sensor able to measure total column amounts of various trace gases, NO_2 included, with absorption cross sections that lie between the Ultraviolet and shortwave infrared spectral regions. Each instrument pixel has a resolution of $3.5 \times 7km^2$ (reduced to $3.5 \times 5.6km^2$ on 6 August 2019 [14]) at nadir, and has little resolution variation at any point on its 2600km swath.

In order to retrieve NO_2 total column amounts, a fitting window of 405-465nm can be used to convert the spectral radiance measured at the top of the atmosphere into slant column density's for each individual pixel. In order to convert this SCD into a tropospheric VCD, first the stratospheric portion of NO_2 is subtracted from the SCD by using global model estimates [1] that are refined using data assimilation. Next, the calculated Air mass Factor (AMF) is used to convert the tropospheric SCD's into VCD's.

Chan et al. [7] validated TROPOMI's NO_2 total columns using a fitting window of 338-370nm. Dimitropoulou et al. [9] used two separate bands to retrieve NO_2 profiles: 425-490nm and 338-370nm which cover NO_2 absorptin of visible and ultraviolet light, respectively. Ialongo et al. [19] and Zhao et al. [51] used a fitting window to validate tropospheric NO_2 columns using a fitting window of 400-440nm.

2.2.5 TEMPO

The Tropospheric Emissions: Monitoring of Pollution (TEMPO) is a satellite borne instrument that will take hourly averaged measurements over the continental United States, including Southern portions of Canada, and extending as far South as Mexico City, and as far East as the Bahamas. The onboard spectrometer has spectral ranges of 290–490nm at a resolution of 0.57nm and 540–740nm at 0.2nm resolution [13]. Each pixel has a ground swath of 2.1km north–south and 4.4km east–west resolution, with simultaneous latitudinal coverage. Every hour, TEMPO will scan east to west along its entire field of view. One of the air quality products from TEMPO will be hourly NO_2 column densities with a resolution of 4x8km with an error budget of $(0.36 \pm 0.2) * 10^{15} \frac{molecule}{cm^2}$ [52]. This error is the result of a sensitivity study where simulated TEMPO radiance spectra and weighting function, using the VLIDORT radiative transfer model, retrieval errors were then calculated using the optimal estimation approach. In order to maintain its FOV, TEMPO will be launched on a geostationary communications satellite, the first instrument of its kind.

Since TEMPO will be the first geostationary instrument to measure NO_2, there is a need to reevaluate analysis methods that were developed for sun synchronous satellites. For instance, Geddes et al. [13] evaluates a new method to separate stratospheric and tropospheric NO_2 column densities. For sun synchronous instruments, separation is rather straight forward. Since the instrument measures the entirety of the Earth, an entire day's measurements could be masked using results from a chemical transport model, which after smoothing would yield an accurate model of stratospheric NO_2, which could be subtracted from the data to retrieve tropospheric column densities. A Geosynchronous satellite, on the other hand, is only limited to its field of view, and using this method alone would leave it vulnerable to transport into and out of its field of view. To overcome this issue, data from outside the TEMPO FOV was also used to provide more context; OMI stratospheric products are used

[5], which have already been modelled according to the previously mentioned method. This new method performs as well as the sun synchronous model, with small biases in the farthest North and South edges of the TEMPO FOV being the only major deviations.

Table 2.1: Summary of DOAS Satellites

Satellite	Launch Date	Pixel Resolution	Orbit Type	Trace Gases	NO_2 Fitting Window
GOME	April 1995	320×40km	Sun-Synchronous	NO_2, BrO, O_3 $OClO, SO_2,$ $HCHO, H_2O$	405-465nm
GOME-2	METOP-A: October 2006 METOP-B: April 2013	80×40km	Sun-Synchronous	NO_2, BrO, O_3 $OClO, SO_2,$ $HCHO, H_2O$	405-465nm
SCIAMACHY	March 2002	30×15km	Sun-Synchronous	NO_2, BrO, O_3 $OClO, SO_2,$ $HCHO, H_2O$	
OMI	July 2004	13×24km	Sun-Synchronous	NO_2, BrO, O_3 $OClO, SO_2,$ $HCHO$	400-450nm
TROPOMI	October 2017	3.5×5.6km	Sun-Synchronous	NO_2, CO, O_3 $CH_4, SO_2, HCHO$	405-465nm
TEMPO	Fall 2022	2.1×4.4km	Geostationary	NO_2, O_3 $C_2H_2O_2, SO_2,$	400-465nm

2.3 Satellite vs ground-based spatial sampling

Differences between ground-based and satellite-based instrumental fields of view can result in the sampling of different air masses. It is expected that spatial and temporal heterogeneity in the distribution of air pollution is present in urban areas and near emission sources, while more rural areas far away from major sources exhibit a more homogeneous distribution of pollution. In order to account for this difference in measured air masses, spatial sampling strategies can be employed to measure an aggregate air volume that is similar to the air volume measured by satellites.

Chan et al. [7] employed a fixed sampling strategy that measured in Munich, Germany between 2016 and 2019. Measurements were performed at 2, 3, 4, 5, 6, 8, 15, 30, and 90° zenith angles at 0, 90, 135, 180, 225, 270, and 315° azimuth angles, relative to true

North; 45° was excluded because the direction was blocked by a nearby building. A single set of measurements took approximately one hour. To retrieve the NO2 profile, a near UV fitting window and the program QDOAS was used. Monthly averages were then compared to monthly averages retrieved from the OMI and TROPOMI satellite sensors, with pixels within 10km of the measuring site being averaged together. On average, satellite measurements underestimated NO_2 concentrations by about 30%. When the ground data was used as a priori profiles for satellite retrieval, the NO_2 VCD's for OMI and TROPOMI increased by 45% and 17%, respectively. This demonstrated that one of the major sources of error in satellite retrieval stems from the coarse spatial resolution of a priori profiles used.

Similarly, Dimitropoulou et al. [9] used a dual scan measuring strategy in Uccle, Brussels. This involved first a vertical scan of 0, 1, 2, 3, 4, 5, 6, 8, 12, 30, and 90° zenith angles at 35.5° azimuth angle relative to due north. This was followed by a horizontal scan with a fixed zenith angle of 2° and at various azimuth angles that were adjusted to improve results, the latest set of directions were 11, 25, 32, 62.5, 105, 262.5, 305, 353, and 344° relative to due north and takes approximately 20 minutes to complete one measuring cycle. Two fitting windows were used for profile retrieval, one in the visible spectrum, and and one in the ultraviolet spectrum. The volume mixing ratios (VMR) of both the UV and VIS spectrum can be used to estimate the distance of the NO_2 peak concentrations, where dL is the differential effective path length:

1. $VMR_{NO_2}^{VIS} > VMR_{NO_2}^{UV}$-The peak concentration is located far away from the measuring site, approximately $dL_{eff}^{NO_2UV} < dL < dL_{eff}^{NO_2VIS}$.

2. $VMR_{NO_2}^{VIS} > VMR_{NO_2}^{UV}$-The peak concentration is located close to the measuring site and is approximately $dL_{eff}^{NO_2UV}$.

3. $VMR_{NO_2}^{VIS} = VMR_{NO_2}^{UV}$ The NO_2 concentration is homogenously distributed along the

line of sight.

This dataset was used to validate TROPOMI columns averaging all satellite pixels that lied within the retrieved effective path lengths and between one hour before and after the TROPOMI overpass time. Comparisons were made between using a set of measurements with a single azimuth direction and the full dual scan measuring strategy and showed an increase in correlation between satellite and ground measurements with an estimated correlation coefficient rising from the 0.25–0.72 range for all seasons to 0.60–0.85; this demonstrates that averaging more azimuth directions result in more accurate validation of satellite profiles.

Ground measurements can also be used to resolve inhomogenities in satellite data. Pinardi et al. [29] used 23 stations that performed MAX-DOAS retrieval at various locations worldwide, as well as 16 Pandora instruments that were performing direct sun retrieval as part of the Pandonia Global Network over differing time periods between 2004 and 2018; retrievals were made within the fitting window of 405–465nm to match satellite windows. Comparisons were made to OMI and GOME-2A satellite data on days with a cloud fraction below 0.5 with satellite data within a 50km radius of each measuring site. To resolve inhomogenities within each satellite's pixels, a dilution correction function was applied to the satellite data set. This radially dependent function was based on ground measurements and described the radial dependence of normalized ground VCD's by dividing the retrieved VCD as a function of radius from the measuring site by c the VCD at the measuring site.

$$F_{dil}(R) = VCD_{NO_2}(R)/VCD_{NO_2}(0) \tag{2.12}$$

The satellite VCD was then divided by the dilution correction function. This function however relies on the assumption that the inhomogenities of tropospheric NO_2 distribution are radial in nature relative to the ground station, which is almost never actually the case. There

is however improved agreement in locations where NO_2 emission is more homogeneously distributed, such as in suburban areas. Regardless, the application of the dilution correction function was able to significantly improve validation results.

Comparisons between ground measurements and chemical transport models can also be used to resolve inhomogenities that satellite data will miss. Ialongo et al. [19] used a comparison between ground based Pandora direct sun measurements and VCD's derived from the CAMS chemical transport model in Helsinki, Finland, 2018. TROPOMI data was averaged within 5km and one hour of the TROPOMI overpass time and a Visible light fitting window was used for ground retrievals, and 405–465 nm for TROPOMI retrievals. In order to resolve tropospheric inhomogenities, the the ratio between the tropospheric VCD retrieved from TROPOMI and the tropospheric VCD retrieved from CAMS was multiplied with the TROPOMI tropospheric VCD as a correction factor; this corrected tropospheric VCD could then be added with the stratospheric VCD retrieved with TROPOMI data to make a corrected TROPOMI total VCD. WHile the total VCD was overestimated at low concentrations of NO_2, the total VCD was underestimated at higher concentrations, which suggests that the stratospheric VCD's retrieved are being overestimated, while tropospheric VCD's are in agreement.

Similarly, Drosoglou et al. [10] also used a chemical transport model to resolve inhomogenities in the Thessaloniki area, Greece between 2014 and 2015. Ground measurements consisted of direct sun measurements and off axis MAX-DOAS offset 80° from the solar azimuth angle, and at 2, 3, 4, 5, 8, 10, 12, 15, 30 and 45° zenith angles; ground measurements were made at three different locations, one rural, one suburban and one urban. To simulate NO_2 VCD's, the CAMx photochemical dispersion model was used, the OMI and GOME VCD's were divided by the simulated VCD's to formulate an adjustment factor, which was multiplied with the satellite VCD's to resolve inhomogenities. For ground measurements, a fitting

window of 400-440nm was used, and satellite pixels within a radius of 25km for OMI pixels and 50km for GOME pixels were averaged together for comparisons. The adjustment factor was shown to improve agreement between ground and satellate data best at the rural site, which suggests it is a good method of resolving inhomogenities that a satellite will miss.

Zhao et al. [51] employed a similar method, however wind data was used to resolve inhomogenities in Toronto, Canada in 2019. Four Pandora ground stations were used, two at an urban site, one at a suburban site and one at a rural site; all took direct sun measurements with a visible spectrum fitting window used for retrieval. Data from the TROPOMI and OMI spacebourne sensors were used, with data between 10 minutes of each satellite's respective overpass time and within 10km of each measuring site was used for validation. The wind data was first used to resample tropomi data by employing a pixel rotation method that aligned each pixel so that the wind direction and two of the ground stations were aligned vertically. Then, the data was resampled along the entire vertical length and 5km horizontally on either side of the vertical. In addition to resolving inhomogenities, this method can analyze NO_2 concentrations that are upwind and will either arrive into the measuring area after satellite overpass, as well as downwind concentrations that have just left the measured region before the overpass. This analysis offsets the need for a sufficiently large sample time, since the data can analyze where concentrations have come and gone, which is convenient since this method requires a sufficiently small sample time to properly resolve changes in wind speed and direction. While this method offered no specific improvement to satellite validation, it was able to resolve local pollution sources as well as regional pollution transport patterns that satellite data would most likely miss.

These previous works suggest that satellite validation improves when ground based instruments measure in more azimuthal directions. The reason for this is quite apparent: let's say that an instrument is performing direct sun measurements next to a busy highway, and

Table 2.2: Summary of DOAS Satellite Validation

	Satellites Validated	Location	Measuring Strategy	Azimuth Angles	Zenith Angles	NO_2 Fitting Window
Chan et al. [7]	TROPOMI, OMI	Munich, Germany	Fixed Azimuth MAX-DOAS	0, 90, 135, 180, 225, 270, 315	2, 3, 4, 5, 6, 8, 15, 30, 90	405-465nm
Dimitropoulou et al. [9]	TROPOMI	Uccle, Brusels	Dual Scan MAX-DOAS	11, 25, 32, 62.5, 105, 262.5, 305, 353, 344	0, 1, 2, 3, 4, 5, 6, 8, 12, 30, 90	425-490nm
Pinardi et al. [29]	GOME-2A, OMI	Global	PGN Composite and Dilution Correction	Various	Various	405-465nm
Drosoglou et al. [10]	OMI, GOME-2	Thessoloniki, Greece (Rural, Suburban, Urban)	Off-Axis MAX-DOAS	80° offset from SAA	2, 3, 4, 5, 8, 10, 12, 15, 30 45	400-440nm
Zhao et al. [51]	OMI, TROPOMI	Toronto, Canada (Rural, Urban, Suburban)	Direct sun and Wind Correction	Direct Sun	Direct Sun	400-4405nm

the SZA throughout the day has the station pointing over the road. The ground station will be measuring emissions from the road exclusively, and with its limited field of view, the ground based instrument will only measure a small portion of the highway at any point in time. However the satellite pixel that measures the road as well will also measure the area surrounding it that is not emitting NO_2. Since the satellite is limited by its field of view in this regard, it is unable to resolve pollution sources within each pixel, instead it sees a composite measurement of all NO_2 that is contained within the square pyramid of atmosphere that lies within the pixel's field of view. It is evident that satellite measurements will appear to be vastly different from ground measurements; the sun only moves 15° every hour which is not enough to cover the highway, let alone the same area as the satellite pixel. Therefore, in order to improve ground-based validation of satellite measurements, a sampling strategy must be developed that can approximately measure a similar air volume as the satellite measurements to be validated.

Chapter 3

Methodology

Passive satellite air quality instruments measure backscattered solar radiation where the retrieval has to account for the photon path down and up through potentially different air masses and over a relatively large area (e.g. for TROPOMI 3.5 x 5.6 km^2 at nadir). Ground-based instruments typically detect photons within a narrow solid angle either by pointing towards the sun or at a limited number of stationary azimuth angles (multi-axis sky scans). The average photon path length in either case depends on the photon wavelength due to molecular Rayleigh scattering and due to Mie scattering by aerosols and clouds. As a result a careful consideration of the sampling differences should be taken into account when using ground based measurements for satellite product validation.

This thesis examines the advantages of a fast multi-azimuthal sky scan approach to satellite product validation with an emphasis on tropospheric column measurements only using the MAX-DOAS technique in 1) rural area (Blacksburg, VA, USA) and 2) heavily polluted metropolitan area (Rotterdam, the Netherlands).

The main instrumentation used in this study to measure NO_2 spatial and temporal distri-

bution is the Pandora spectroscopic system described in Sec (2.1.6). The main approach consists of fast measurements at 3 elevation angles (15^o, 30^o and 90^o) and at multiple fixed azimuth angles relative to the Sun (on both "sides" of the Sun). The main motivation for the offset from the Sun ($> 60^o$) is to reduce retrieval dependency on the knowledge about the aerosols at small relative azimuth angles.

The following sections will describe in detail the methodology to evaluate the effect of spatial sampling on satellite validation:

Rural Blacksburg, VA, USA:

- Location and instrumentation
- Measurement schedule
- Data analysis: 1) DOAS fitting; 2) Direct sun total column analysis; 3) MAX-DOAS tropospheric column analysis (including VCD calculation, estimation of horizontal path and cloud screening); 4) comparison between tropospheric columns from 2 observation geometries; 5) temporal and spatial variability; 6) comparison between observation variability and satellite NO_2 measurement precision.

Urban polluted Rotterdam, the Netherlands:

- Location and description of TROLIX-19 campaign
- Measurement schedule
- Data analysis: 1) DOAS fitting; 2) MAX-DOAS tropospheric column analysis (including VCD calculation, estimation of horizontal path and cloud screening); 3) temporal and spatial variability simulated by a chemical transport model (including description of the model); 4) effect of volume sampling on MAX-DOAS and satellite measurements

using chemical transport model simulations 5) comparison between MAX-DOAS observation variability and satellite NO_2 measurement precision.

3.1 Measurements at rural Blacksburg, VA, USA

3.1.1 Location

Blacksburg, VA is a rural location, home to the Virginia Polytechnic Institute and State University (Virginia Tech). The main sources of pollution are local traffic, highway traffic (interstate-81 and state-460) university power generation, regional transport and Radford Army Ammunition Plant (located about 15 km South-West from Blacksburg).

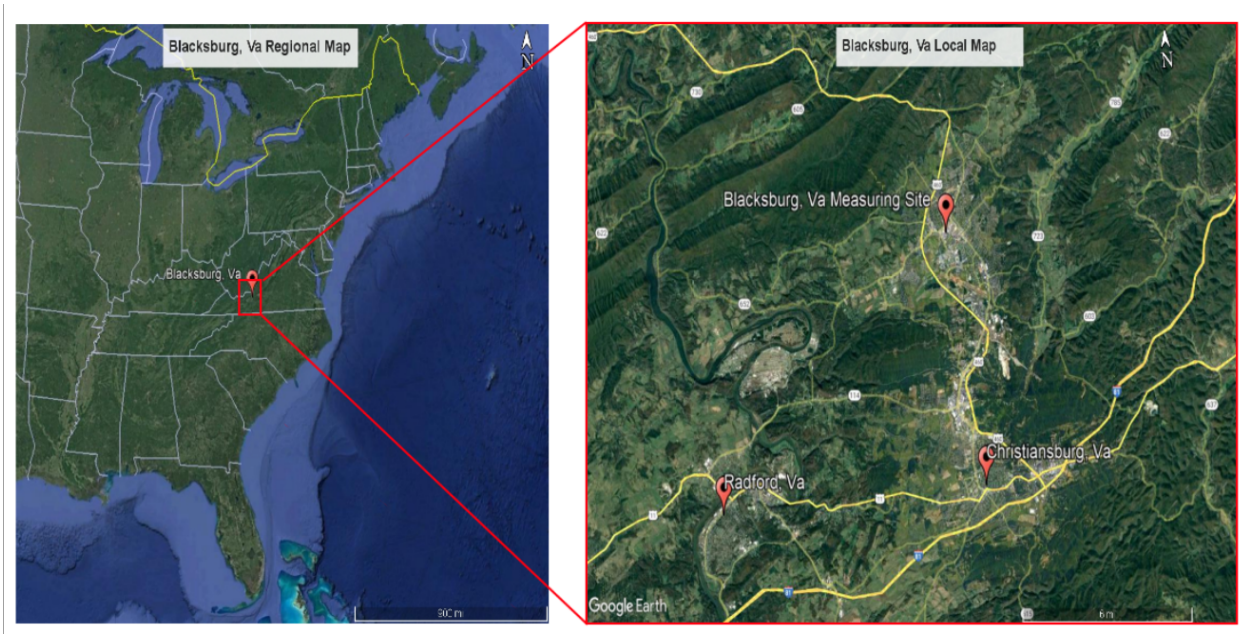

Figure 3.1: Regional and local maps depicting the area around the measuring site

The instrumentation was installed on the roof of Whittemore Hall (37.230774°, −80.42468°, 690 m above see level) on the Virginia Tech campus, Blacksburg, VA, USA. The building is 6 stories tall and a 7th story penthouse that blocks sky views between $350^o - 60^o$ azimuth

angles (from North).

Figure 3.2: Panoramic view of the sky line from the measurement location on the Whittemore Hall roof (Virginia Tech) in Blacksburg, VA, USA.

3.1.2 Instrumentation

To evaluate spatial and temporal heterogeneity of NO2 distribution and satellite validation sampling strategy three Pandora spectroscopic instruments (Pandoras 148, 168, 188, SciGlob) were simultaneously deployed from the same location.

A full sky camera (Schreder-CMS, ASI-16) was recording sky conditions every 2 min to ensure cloudy conditions are excluded from the dataset. Images are taken every 2 minutes from two hours before sunrise to two hours after sunset at two different exposure times: one normal and one underexposed, and are automatically uploaded to an ftp server to be downloaded and processed later. Before processing, the images are all mirrored, in order to change the image from an upward looking image to a ground based image [37]. In addition, the images are offset by 25° in order to properly align them due East, and the vertical FOV is limited to nadir to 20° above the horizon.

Meteorological fields (temperature, pressure, relative humidity, wind speed and wind direction) were monitored by the Vaisala weather transmitter (WXT 520).

3.1.3 Measurement Strategy

The measurement strategy was to capture spatial heterogeneity at high temporal resolution. Considering that to achieve an acceptable signal-to-noise ratio solar spectra need to be averaged over 20-30 sec three instruments were used in unison to sample various directions and air masses. Pandora 168 took direct sun measurements (total column) to provide total column high temporal resolution measurements (every 1 min)

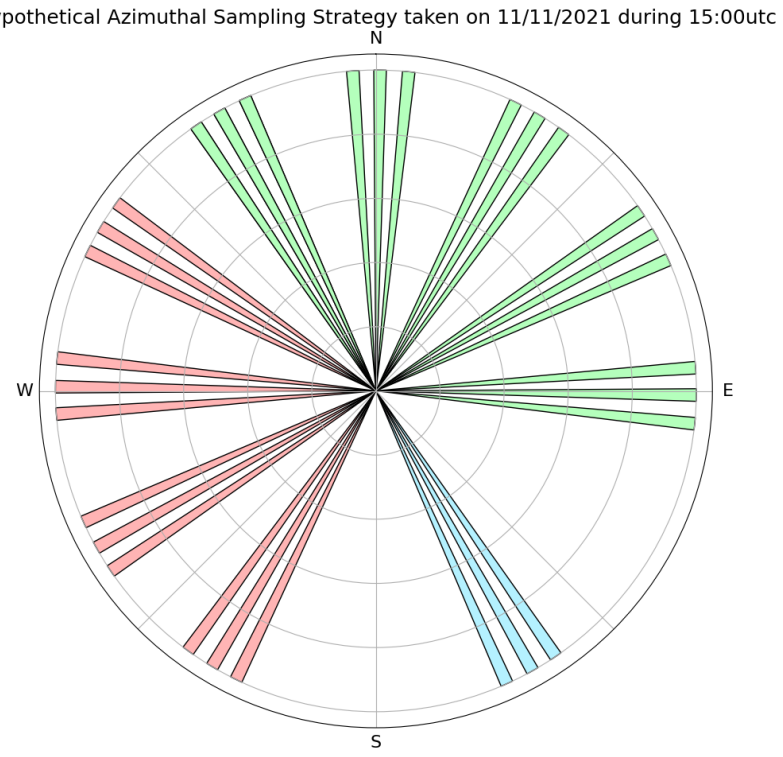

Figure 3.3: Example of measurement strategy taken by Pandora 148 and 188 during 14:30 - 15:30 UTC on 11/11/2021. The red bars correspond to Pandora 148, the green are measurements taken by Pandora 188. The three blue bars represent the solar azimuth angle at the start of each measurement cycle and measured by both instruments and P168 in continuous mode

Pandoras 148 and 188, on the other hand, were set to take sky measurements inter dispersed

with direct sun measurements. Scattered sky hyperspectral visible measurements were taken at $2°, 60°, 75°, 60°$, and $2°$ zenith angles in a V-time sequence at $60°, 90°, 120°, 150°$ and $180°$ offset from either side of the sun. This approach allows for the two measurements on either side of the highest zenith angle measurement (where most of information is coming from) be used to evaluate atmospheric scattering conditions changes and averaged to improve measurement precision. One vertical scan takes place about 3 min. One cycle takes approximately 20 minutes to complete, and was repeated 3 times in an hour from sunrise to sunset

Figure 3.3 shows the azimuth distribution of this sampling schedule over 1 hr. This allows for an even azimuthally distributed set of measurements to be taken every hour, and is dynamic enough to avoid losing samples due to the proximity to the sun position. It also samples the entire 360^o over the duration of a day allowing for full spatial coverage for validation of Geo-stationary satellite products.

3.2 Data Analysis

3.2.1 DOAS Fitting

Differential slant column densities, total and tropospheric columns of NO_2 (and O_2O_2) were calculated using the BlickP (Version 1.8.16) software ([6]).

Direct sun total columns were determined from visible spectra using the nvs3 r-code that corresponds to the following fitting settings: (f-codes: nvs4, nvs5), Vandaele et al. [46] 220k NO_2 for the nvs4 r-code, and the same cross section at 230K for the nvs5 r-code, Serdyuchenko et al. [38] 293K O_3, Thalman and Volkamer [42] 295K O_4, and Rothman et al. [35] H_2O absorption cross sections at a fitting wavelength window of 400-470nm,

broad band absorption was fitted using a 4th order polynomial, and a 1st order wavelength shift polynomial, 0th order offset correction polynomial, and oth order resulution change correction polynomial were used as well. The reference spectrum was taken on 3-May-2022.

MAX-DOAS tropospheric columns were calculated from spectra collected without filters using the nuh1 r-code that corresponds to the following fitting settings: (f-code: nuh1) Vandaele et al. [46] 294k NO_2, Serdyuchenko et al. [38] 293K O_3, Meller and Moortgat [27] 298K $HCHO$, and Thalman and Volkamer [42] 295K O_4 at a fitting wavelength window of 336-370nm, broad band absorption was fitted using a 5th order polynomial, and a 1st order wavelength shift polynomial, and 1st order offset correction polynomial were used as well for MAX-DOAS analysis.

3.2.2 Direct Sun NO_2 Total Column Analysis

Estimation of the amount in the reference spectrum: In order to convert ΔSCD retrieved during DOAS to vertical column densities, the NO_2 SCD in the reference spectrum (SCD_{ref}) first must be estimated (Eq. 3.1).

$$VCD_{total} = VCD_{trop} + VCD_{strat} = \frac{\Delta SCD + SCD_{ref}}{AMF_{DS}} \tag{3.1}$$

SCD_{ref} was determined using Modified Langley Extrapolation method for Pandora 148 by Dr. Elena Lind. The rest of the Pandoras (188 and 168) were intercalibrated to Pandora 148 total columns. Figure 3.4 shows agreement between NO_2 total columns on 19-Nov-2021.

Air Mass Factors were calculated by BlickP based on solar zenith angle and troposphere-stratosphere profile distribution according to Eq. (2.5)

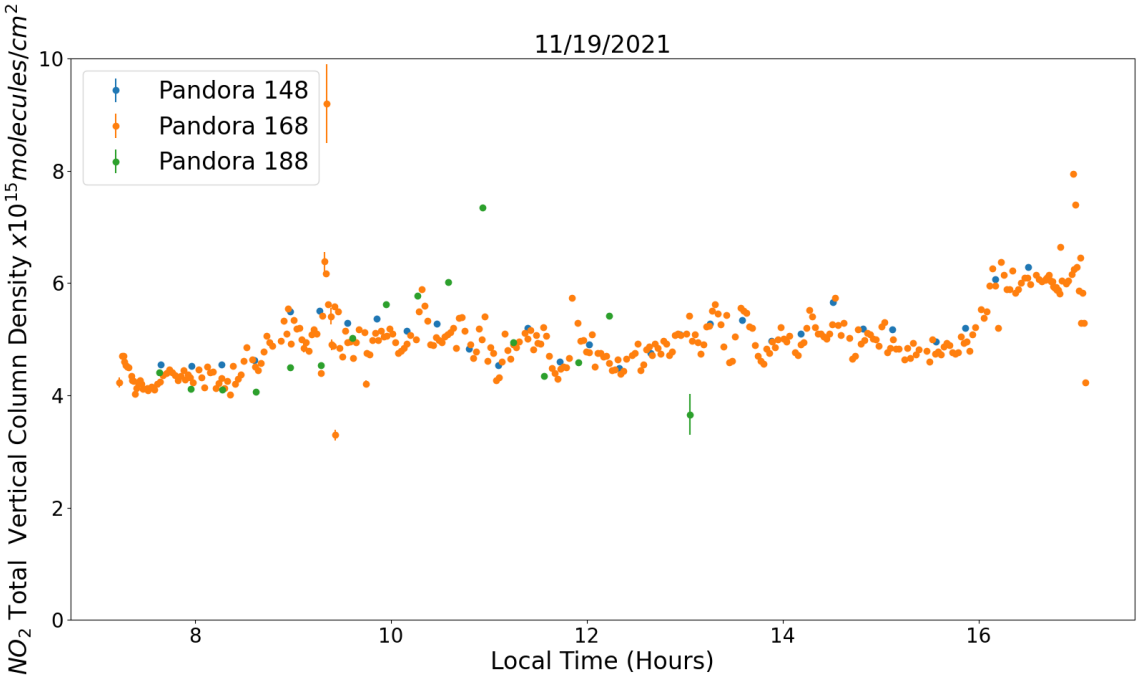

Figure 3.4: Retrieved calibrated Slant Column Densities and uncertainties for the three instruments on 19-Dec-2021

Estimation of stratospheric column: This data product represents the total vertical column density through the atmosphere, since direct sun measurements are sensitive to both tropospheric and stratospheric trace gas profiles, however, the tropospheric vertical column density is a more applicable data product in the context of air quality measurements, since stratospheric air does not affect the quality of air breathed by people. While not directly measured, the stratospheric component of the total vertical column density can be estimated through three approaches. 1) Derive stratospheric NO_2 during morning and evening twilight hours from zenith sky measurements and use chemical box model to estimate date time NO_2 column ([32]); 2) use temperature dependence of NO_2 molecular absorption cross section [40]; 3) estimate $NO2$ from climatology, where satellite measurements of NO_2 are used to model the effects of meteorological conditions such as air pressure and temperature as well as aerosol properties on stratospheric NO_2 profiles. This model can then be used to estimate

the stratospheric profile of NO_2 knowing only climatological properties. In this work the 3rd approach was used. BlickP estimates climatological NO_2 profiles based on the work Brohede et al. [4], where DOAS retrievals from the Osiris satellite-based instrument are used to determine stratospheric NO_2 profiles using the LIMBTRAN chemical transport model. This model can be used to estimate the stratospheric vertical column density of NO_2 based on latitude, time of day, and season of the year.

Data filtering and averaging: In order to ensure only high quality direct sun retrievals are used only measurements with a DOAS fitting residual optical depth root mean squared below the median for the entire dataset are used. This will discount measurements where the sun is obscured by clouds and when spatial stray light is impacting the photon path (e.g. at high solar zenith angles). Next, temporally coincident measurements ($<$ 10 minute) from the three instruments are averaged together, these measurements are of the exact same air volumes, and any difference in retrievals comes from error. Next, measuring cycles with more than 10 valid measurements, which corresponds to an average maximum time between measurements of 6 minutes, are interpolated, in order to determine the minute by minute vertical column density. This interpolation will give a more complete picture of the atmosphere that is measured each cycle, and therefore will improve comparisons between the two measuring strategies. Since the data are analysed for the purpose of Geostationary satellite products measurements are averaged over 1 hr.

3.2.3 MAX-DOAS Tropospheric Column Analysis

The MAX-DOAS tropospheric vertical column densities were calculated using BlickP from the retrieved differential slant column densities using the following equation [6]:

$$VCD_{trop} = \frac{\Delta SCD_{75^\circ} \cdot VCD_{O_2O_2}}{dSCD_{75^\circ,O_2O_2} - \Delta SCD_{60^\circ,O_2O_2} + 2 \cdot VCD_{O_2O_2}} \tag{3.2}$$

Where $dSCD_{75^\circ,O_2O_2}$ and $dSCD_{60^\circ,O_2O_2}$ are the differential slant column densities of O_2O_2 for 75° and 60°, respectively, and $VCD_{O_2O_2}$ is the climatological estimation of the total vertical column density of O_2O_2, which can be determined through meteorological measurements of air pressure and temperature. After calculation of the tropospheric vertical column density, quality is assured through the analysis of measurement uncertainty, which has been identified as a more accurate representation of measurement quality [21] than the rms of the DOAS fit, as was applied for Direct Sun measurements. Measurements with an uncertainty greater than 30% of the measurement are discarded. Finally, these measurements can be averaged together to provide a spatial and temporally averaged tropospheric vertical column density for the measuring cycle.

Estimation of photon path length: To better characterize the sampled air volume an estimation of the photon path has to be made. Horizontal and vertical components of the average light path of the sky scattered photons can be estimated using a single scattering approximation and O_2O_2 absorption. This approach will provide a maximum length since the true nature of radiative transfer processes in the atmosphere is multi-scattering.

$$L_{O_2O_2}(\lambda, VZA, RAA) = \frac{\Delta SCD_{O_2O_2}(\lambda, VZA, RAA)}{c_{O_2O_2}^{surface}} \tag{3.3}$$

Equation 3.2.3 estimates the path length for a specific observation geometry and wavelength ($L_{O_2O_2}(\lambda, VZA, RAA)$) for O_2O_2 relative to the surface concentration of O_2O_2 [48]. Technically, the effective concentration of O_2O_2 profile for the specific observation geometry and

scattering conditions should be used but it is typically not known (it requires the prior knowledge of the sampling volume) In addition this estimation most likely does not represent the path through the NO_2 layer since the majority of tropospheric NO_2 resides much closer to the surface than O_2O_2. This will lead to a path length with a maximum height well above the top of the NO_2 near surface layer.

3.2.4 Cloudy data filtering

To exclude any contamination of the ground-based data analysis by the cloud effects on scattering and retrieval cloud covered sky fraction was determined from the full sky RGB images as shown in 3.5

Figure 3.5: A typical skycam image taken at the Virginia Tech ground station on 11/15/2021 at 9:00 before mirroring and offset correction.

The Schreder-CMS ASI-16 is a fisheye imager, pointed at the sky, able to take RBG images of the full sky, with a FOV of 360° horizontally and 90° vertically, however due to distortions

around the horizon in sky images that can affect image analysis only 70° from the vertical in each sky image is analyzed.

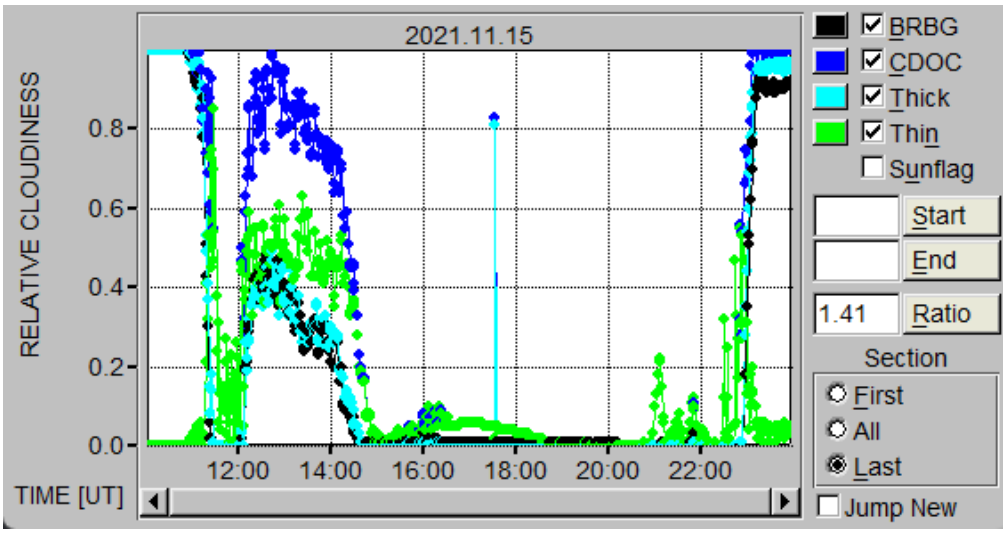

Figure 3.6: Time Series of cloud fractions calculated for 11/15/2021. Times are in hours UTC, and the CDOC plot represents the sum of the thick and thin clouds calculated.

In order to analyze each sky image, two algorithms are employed using the Findclouds sky image analysis software developed by CMS-Schreder. As a first pass of any image, the BRBG (Brightness Red Blue Green) algorithm checks the ratio of blue/red+blue/green over the entire image. Next, every combined pixel ratio is compared to a preset ratio for clouds, and every pixel ratio under this value is considered covered by clouds. Next, the underexposed image is analyzed in the same manner, except now these pixels are used to smooth areas around the clouds as well as the sun to get a more realistic analysis of cloudiness. The cloud fraction itself is computed by taking the fraction of pixels after smoothing that are considered covered by clouds.

Next, the Cloud Detection and Opacity Classification (CDOC) algorithm builds on BRBG analysis by comparing images confirmed to be clear of clouds to images to be analyzed. To begin, a clear sky library is developed using images that have a cloud fraction of less than 0.01 as determined by the BRBG algorithm, and confirmed by user inspection, about a day's

worth of images is sufficient for analysis. Figure 3.6 shows the results of both algorithms on 11/15/2021. For Figure 3.5, the calculated cloud fractions were 0.25 for the BRBG algorithm, and 0.76 for the CDOC algorithm. The clouds in Figure 3.5 cover a majority of the image, which is closer to the results of the CDOC algorithm. In addition, the BRBG algorithm's result coincides with the calculated cloud fraction of thick clouds in the image, however, it is not able to detect the thin clouds that the CDOC can. Therefore, only CDOC results will be used to determine cloud free days. Cloud fraction below 20% is considered cloud free. The total number of cloud free days used in this work was 30.

3.2.5 Comparison between tropospheric NO_2 columns from direct sun and multi-axis observations

The following datasets were generated during the previous stages:

1. Mean and standard deviation of tropospheric columns over all MAX-DOAS azimuth directions during 1 hr period;
2. Mean and standard deviation of total columns from direct sun measurements during 1 hr period;
3. Mean and standard deviation of tropospheric columns calculated from direct sun total column measurements and stratospheric column climatology-box model estimation during 1 hr period.

To evaluate spatial homogeneity and measurements consistency difference between tropospheric columns derived from direct sun and multi-axis was calculated (both absolute and relative). A seasonal offset between the direct sun and multi-axis tropospheric NO_2 columns can be indicative of stratospheric correction issues.

3.2.6 Evaluation of spatial homogeneity in rural locations and its implications for satellite validation

In environments with a homogeneous air pollution distribution, both direct sun and multi-axis measurements should produce the same columns (within their corresponding errors), if stratospheric component is subtracted correctly from the total column. Standard deviation of the measurements from 8 multi-axis azimuth angles within 1 hr should be representative of the measurement precision and spatial heterogeneity. If standard deviation of the multiple azimuth angle measurements is equal to standard deviation of the direct sun measurements the conclusion is that the area is relatively spatially homogeneous and only one direction (e.g. direct sun or single azimuth sky scan) might be sufficient for validation purposes. If this is not the case, the measured standard deviation from multiple direction measurements should be compared to the satellite tropospheric column total error. If the satellite errors are larger than the detected variability, again, only one direction might be sufficient. If the satellite errors are comparable or smaller, multi azimuth angle measurement strategy can be recommended for validation purposes.

3.3 Measurement in urban polluted Rotterdam, the Netherlands

3.3.1 TROLIX'19 Field Campaign

The TROLIX'19 (TROpomi vaLIdation eXperiment 2019) was a multi-agency, multi-institution field campaign (4-Sep to 4-Oct-2019) led by the Royal Dutch Meteorological Institute (KNMI). The main goal of TROLIX'19 was validation of TROPOMI L2 main data products includ-

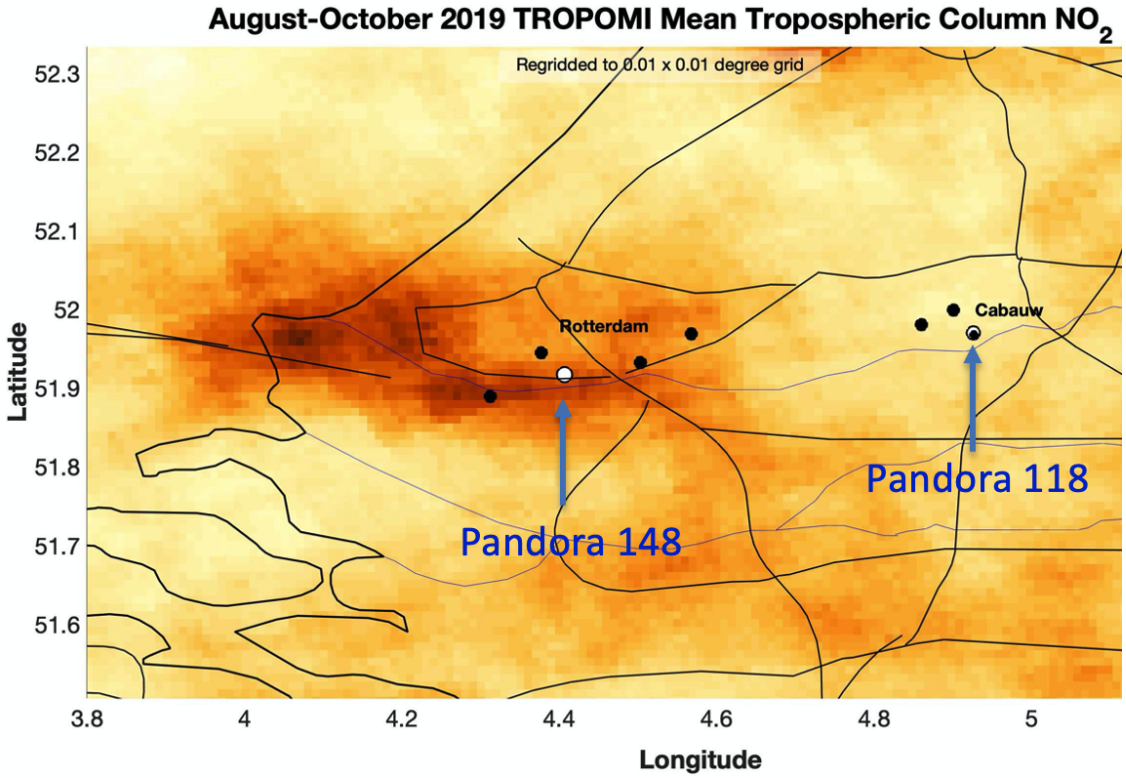

Figure 3.7: Mean tropospheric column NO_2 for August-October 2019 derived from TROPOMI measurements. Data have been re-gridded onto a $0.01^o x 0.01^o$ grid for the calculation of the 3 month mean.

ing UVAI, Aerosol Layer Height, NO_2, O_3, and $HCHO$ under a wide range of atmospheric conditions. To characterise sub pixel heterogeneity effects local networks of sensors were deployed around rural Cabauw (51.97° N, 4.93° E) and within the densely populated industrial city of Rotterdam, the Netherlands during TROLIX'19.

Measurements made during the campaign include in-situ surface, sonde (O_3 and NO_2) and airborne, satellite-based and ground-based remote sensing (LIDAR, DIAL, sun photometer, scanning spectrometer instruments). This work focuses on tropospheric column measurements by Pandora 148 located in Rotterdam (see Fig. 3.7). In addition, air pollution was modeled using the LOTOS-EUROS (Long Term Ozone Simulation European Operational Smog) model at $1x1km^2$

3.3.2 Measurement Schedule

Pandora 148 was deployed from 1 September to 4 October, 2019 on the roof of a three-story building in Schiedam, located in the Rotterdam–The Hague metropolitan area, west of Rotterdam (51.9172^o, 4.4066^o, 7 m above sea level). Only two azimuth directions had a proper clearance for full MAX-DOAS scans: 261.5^o (MAX-DOAS measurements from 2019/09/04: 1, 2, 3, 4, 5, 6, 8, 10, 15, 30, 88^o elevation angles), and 54.5^o (MAX-DOAS measurements from 2019/09/21: 1, 2, 15, 30, 88^o elevation angles). In addition to the fixed azimuth angle scans, observation at azimuths relative to the solar azimuth angle were performed: $\pm$90, $\pm$135^o at only three elevation angles (15, 30, 88^o) to measure tropospheric column heterogeneity around the site (from 2019/09/04). Multi-axis measurements were inter dispersed with direct sun observations (from 2019/09/01 - 2019/10/04) where 2 measurements were taken without any filters (open) and two with U340 filter/diffuser combination. Each direct sun measurement was about 40 sec. Measurements in all directions were done sequentially changing filter wheel positions from open to U340 filter. Total integration time per elevation angle for fixed azimuth directions was 15 sec for measurements taken with no filters (open), and 20 sec for measurements taken with U340 filter. Measurements at 1^o elevation angle were done at 30 sec for open and 40 sec for U340 spectra. All varying zenith angle measurements were taken at 40 sec total integration times. About 15% of the total integration time was devoted to the dark measurements. The full sequence (4 full MAX scans in 261.5^o direction, 2 partial scans in 54.5^o direction, 4 relative to the sun azimuth partial scans and 10 direct sun measurements) took about 53 minutes. No dedicated time was given to the zenith only measurements for reference generation around local noon. Since measurements in zenith direction were done before and after each partial and full scans significant number of spectra are available for the reference creation

3.3.3 Data Analysis

MAX-DOAS Tropospheric Column Analysis: NO_2 differential slant column densities were calculated using QDOAS software (v.) by Dr. Elena Lind and the data processing procedures established during CINDI-2 [21] in UV spectral window. Tropospheric Vertical Column Densities of NO_2 were determined in the same way as discussed in Sec 3.2.3. The tropospheric VCDs were temporally averaged over one hour period in the same manner as measurements taken in Blacksburg, VA, in order to show the effects of spatial heterogeneity in a polluted environment. While the measuring strategy used in Rotterdam does not have as many spatially distributed measurements (5 azimuth angles vs 10), there are enough to show in general how spatial averaging affects validation.

Spatio-temporal Variability Analysis using the LOTOS-EUROS Chemical Transport Model: The Long Term Ozone Simulation(LOTOS) European Operational Smog (EUROS) [25], or LOTOS-EUROS chemical transport model was used to simulate NO_2 vertical concentration profiles within the TROLIX'19 domain during the duration of campaign. This run of LOTOS-EUROS is an experimental run with horizontal resolution of 1 x $1km^2$ and 12 vertical layers (maximum height: 9500m with 20m-2500m layer depths), which have been provided by the Netherlands Organization for Applied Scientific Research.

Estimation of effective profiles along the photon path: ground-based measurements Using these simulated $NO2$ concentration profiles, the sensitivity of the ground-based observations can be evaluated as a function of sampling direction and distance. In this work a single scattering approximation is used to estimate average photon slant path based on O_2O_2 ΔSCD at 75^o viewing zenith angle (same as in Eq. 3.2.3 for tropospheric column). An "effective" NO_2 number density profile (n_i) along the slant photon path was estimated

by weighing each model cell layer volume mixing ratio ($\chi_{i,j}$) by the path fraction through that layer ($f_{i,j}$) according to Eq. 3.4. This approach provides a simple characterization of the "integrated" heterogeneity "seen" by the Pandora ground-based instrument.

$$n_i = \sum_j f_{i,j} \cdot \frac{\chi_{i,j}^{NO_2} \cdot P_{i,j}}{k_B T_{i,j}} \tag{3.4}$$

Where i is the integer layer height, from 0 to 12, j is the integer LOTOS-EUROS cell number along the estimated path length, P is an average layer pressure (interpolated in log scale) in Pa, and T is the average layer temperature in K, and k_B is the Boltzmann Constant: $1.3807 \times 10^{-23} JK^{-1} molecule^{-1}$.

Estimation of effective profiles along the photon path: satellite-based measurements. A similar approach can be employed to simulate the "effective" vertical profiles that are "seen" by TROPOMI detected photons. In this study it is assumed that the downwelling and upwelling paths of the photons will encounter the entire atmosphere equally (single scattering approximation ignoring actual weighting functions) within the ground-level pixel foot print. This is done by finding the percentage of each LOTOS-EUROS box that resides inside of a relevant TROPOMI pixel, and summing each cell's NO_2 contribution at each layer The tropospheric Vertical Column Densities for both ground and satellite measurements can be determined by integrating the simulated profiles from the surface to the top of troposphere.

Effect of Spatial Sampling on MAX-DOAS and Satellite Measurements: To show the effect of spatial sampling on measurements through the LOTOS-EUROS model, both the simulated profiles and VCDs of ground-based and satellite-based platforms can be compared to each other. Differences in profiles correspond to spatially heterogeneous NO_2 concentrations, which will show the effect of measuring different air volumes in an inhomogeneous

environment on satellite validation. In addition, the estimated path lengths can be compared to satellite pixel size to demonstrate how the range and direction of ground-based measurements affects their relevancy in satellite validation at a particular measuring site. Finally, the simulated profiles can be integrated by the height to determine each corresponding tropospheric vertical column density, which can be compared to the real measured vertical column densities to evaluate model accuracy.

Chapter 4

Results

4.1 Blacksburg, VA NO_2 observations

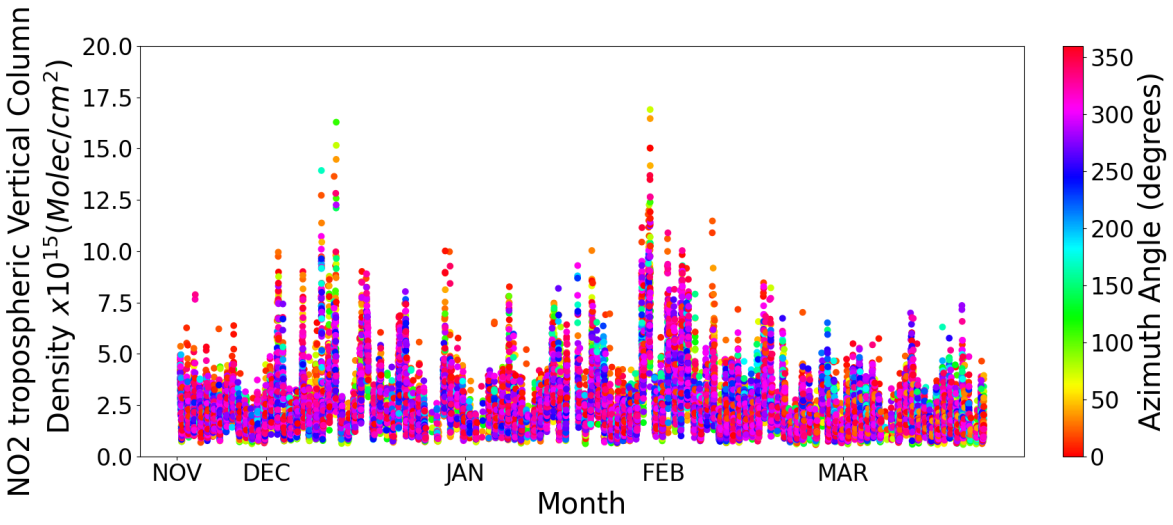

Figure 4.1: Tropospheric NO_2 VCD's retrieved since 11/16/2021 from both Pandora 148 and 188. The color of each point is dependant on the azimuth viewing angle.

Figure 4.1 shows the time series of NO_2 tropospheric VCD for the entire measuring period. For most of the measuring period the NO_2 tropospheric columns ranged between

$(1-5) \times 10^{15}[\frac{molecules}{cm^2}]$ with an average of $2.57 \times 10^{15}[\frac{molecules}{cm^2}]$ and a standard deviation of $1.536 \times 10^{15}[\frac{molecules}{cm^2}]$, which is consistent for measurements in low pollution rural locations [10]. Larger tropospheric NO_2 columns were also observed suggesting transport and local contributions that are above background level.

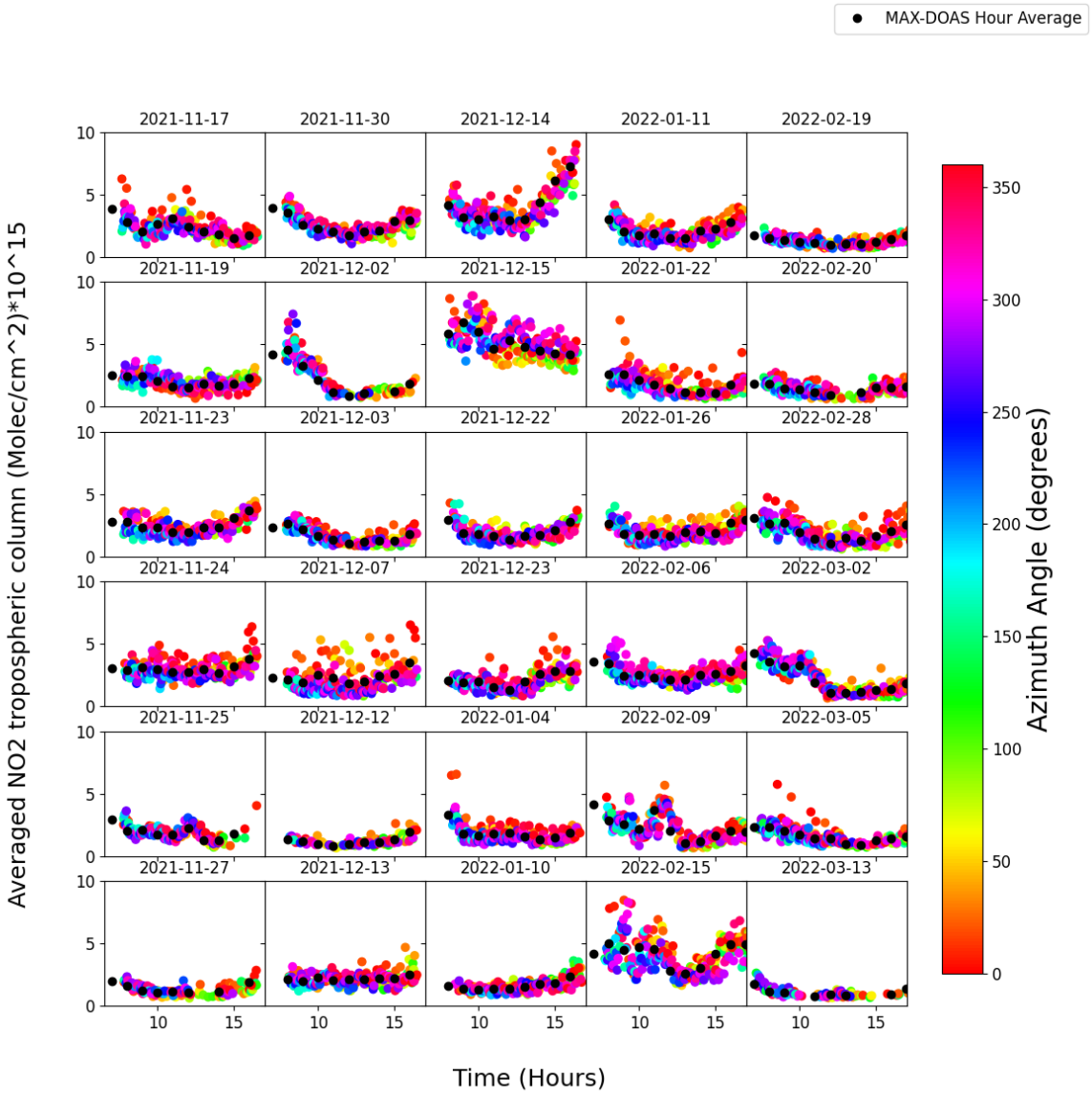

Figure 4.2: Time series NO_2 tropospheric vertical column densities for days with low cloud fractions. Black points correspond to the averaged MAX-DOAS values from the previous hour, and the color of each point is dependant on the azimuth viewing angle. Time is measured in hour in hours UTC

Figure 4.2 shows the original time series of NO_2 tropospheric columns for cloud free days, as well as the 1 hr averaged VCD from all azimuthal directions. Here the variability due to azimuth angle is more clear. Each hourly average shows the net change in tropospheric VCD in the Blacksburg area. On December 14, for instance, increased traffic due to students leaving the University at the end of the semester led to increased columns detected between 250° and 300°, which corresponds to one of the major routes out of Blacksburg, when compared to other days when daily traffic was not as high. However the spatial variability is reduced after averaging, with the averages for each measuring cycle detailing how NO_2 levels varied hour by hour in the Blacksburg area as a whole, as opposed to variability in a single direction.

Figure 4.3 shows the hourly averaged MAX-DOAS and direct sun tropospheric columns for the entire measuring cycle, as well as the absolute and percent differences between the two data sets, respectively. In addition, the average uncertainties of each measuring cycle are included as error bars. Since Direct Sun measurements measure unscattered sunlight and have a higher signal to noise ratio than MAX-DOAS measurements,the average uncertainty of each measurement is smaller in comparison; however the uncertainty in the climatological estimate of the stratospheric NO_2 vertical column density is on average six times larger than the measurement uncertainty ($0.27 * 10^{15}$ vs $0.043 * 10^{15}[\frac{molecules}{cm^2}]$) and is the main contributor to estimation of direct sun tropospheric column measurement uncertainty. The average absolute difference between direct sun and MAX-DOAS tropospheric columns is $5.07*10^{14}[\frac{molecules}{cm^2}]$ with a standard deviation of $4.2*10^{14}[\frac{molecules}{cm^2}]$. Direct Sun overestimated MAX-DOAS tropospheric vertical column densities by approximately 30% at a standard deviation of 27%. However, the interpretation of this should be done with care since the actual tropospheric columns are very small and the difference is close to the measurement error. The low variability between the two types of measurements suggests that the area

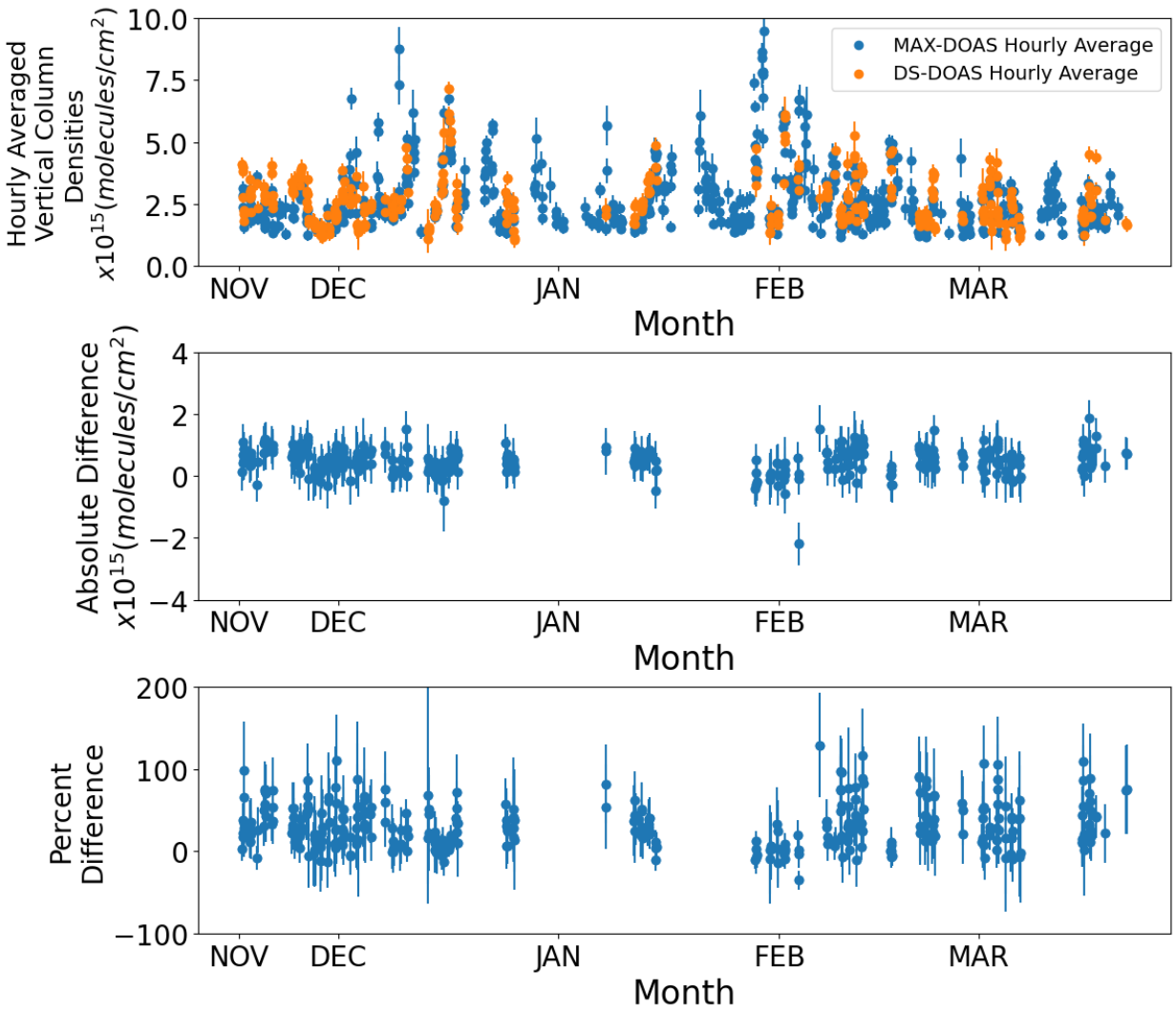

Figure 4.3: (a) MAX-DOAS and direct sun tropospheric VCDs throughout the measuring Period (1hr averaged); (b) The absolute difference between DS and MAX-DOAS hourly averages; (c) Percent difference between DS and MAX-DOAS hourly averages. The error bars represent a) absolute measurement uncertainty for tropospheric vertical column densities retrieved from both viewing geometries, b) the sum of the absolute uncertainty from temporally coincident MAX-DOAS and Direct Sun measurement cycles, and c) the percent error between measurement cycles.

has a relatively homogeneous distribution of NO_2. Since NO_2 distribution is relatively homogeneous around Blacksburg, the direction of the observations is not as important for satellite validation. This is consistent with results from Drosoglou et al. [10] and Zhao et al.

[51] which showed improved validation results of satellites in rural areas with lower NO_2 pollution as opposed to urban areas with higher NO_2 levels. The percent decrease matches the 30% seen in other works [7].

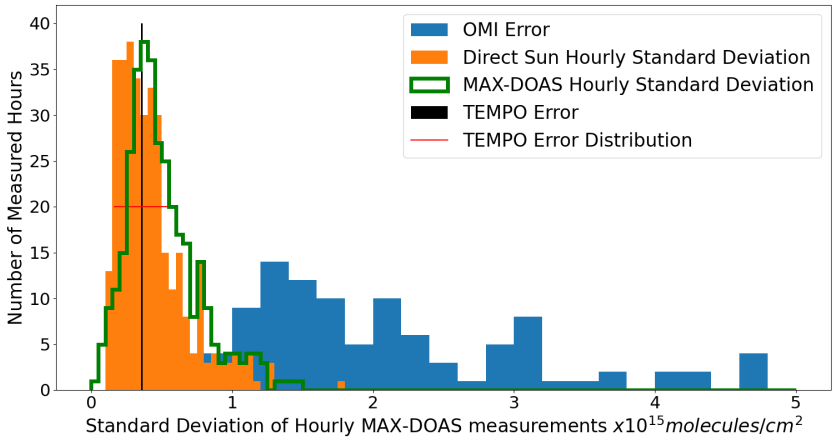

Figure 4.4: Histogram depicting the standard deviation of the hourly MAX-DOAS and Direct Sun measurements as well as histograms for OMI errors during the measuring period. The theoretical error and precision of TEMPO is depicted by black and red lines, respectively.

The effects of low pollution and homogeneity can be further seen in Figure 4.4. Here the standard deviations of MAX-DOAS and Direct Sun hourly averages were overplotted on OMI errors during the same measuring period. In addition, the theoretical error for TEMPO NO_2 retrievals is represented by the black bar, with its upper and lower bounds represented by a red error bar. Due to the homogeneous distribution of NO_2 around Blacksburg, the distribution of standard deviations of MAX-DOAS and Direct Sun hourly averaged data sets are very similar. This means that the measurements taken in a single direction "see" similar variability to measurements of a larger air volume. In order to properly validate satellite measurements, a measuring strategy should be developed that will have a higher distribution of standard deviations to the error of satellite measurements. Figure 4.4 also demonstrates the effectiveness of the measuring strategy for two different satellites. Assuming the error of

TEMPO measurements will coincide with its theoretical limits, both Direct Sun and multi-azimuth angle measuring strategy would be needed for TEMPO to more accurately validate TEMPO. This is because the inhomogeneities measured on the ground match the proposed error for TEMPO. This means that the inhomogeneities measured on the ground would be measured by TEMPO as well, and cannot be discounted as the result of error. On the other hand, OMI, due to its older design and larger ground pixel size, has larger errors. This means that the inhomogeneities measured will not affect OMI retrievals, instead the inhomogeneities will be overshadowed by error.

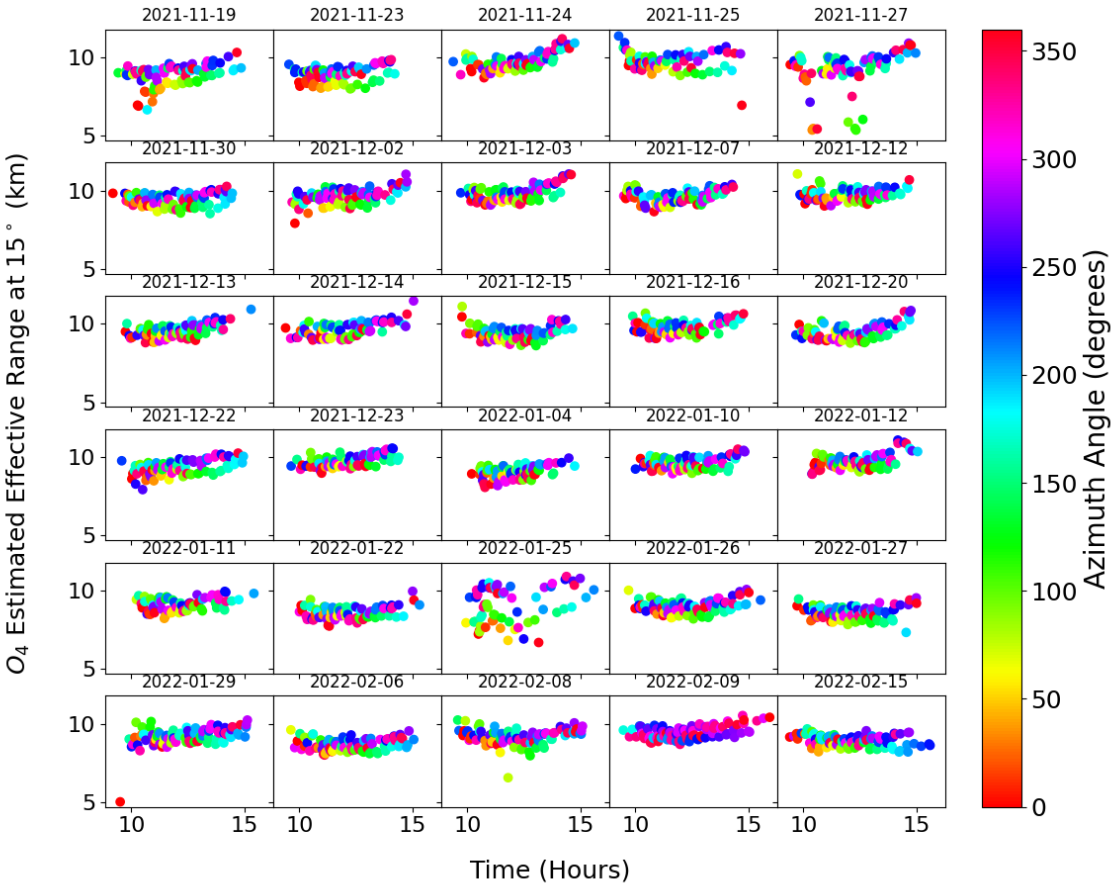

Figure 4.5: The MAX-DOAS estimated maximum range of the O_2O_2 scattering altitude for 30 clear days during the measuring period at a Measuring Zenith Angle of 15°.

Finally, Figure 4.5 shows the maximum estimated range of measurements taken in Blacksburg at a 15° measuring zenith angle on cloud free days. These values remain consistently around 10km; this means that the furthest NO_2 concentrations that are measured in Blacksburg are approximately 10km away, which corresponds to an estimated height of approximately 2.5km.

4.2 Rotterdam, the Netherlands NO_2 observations

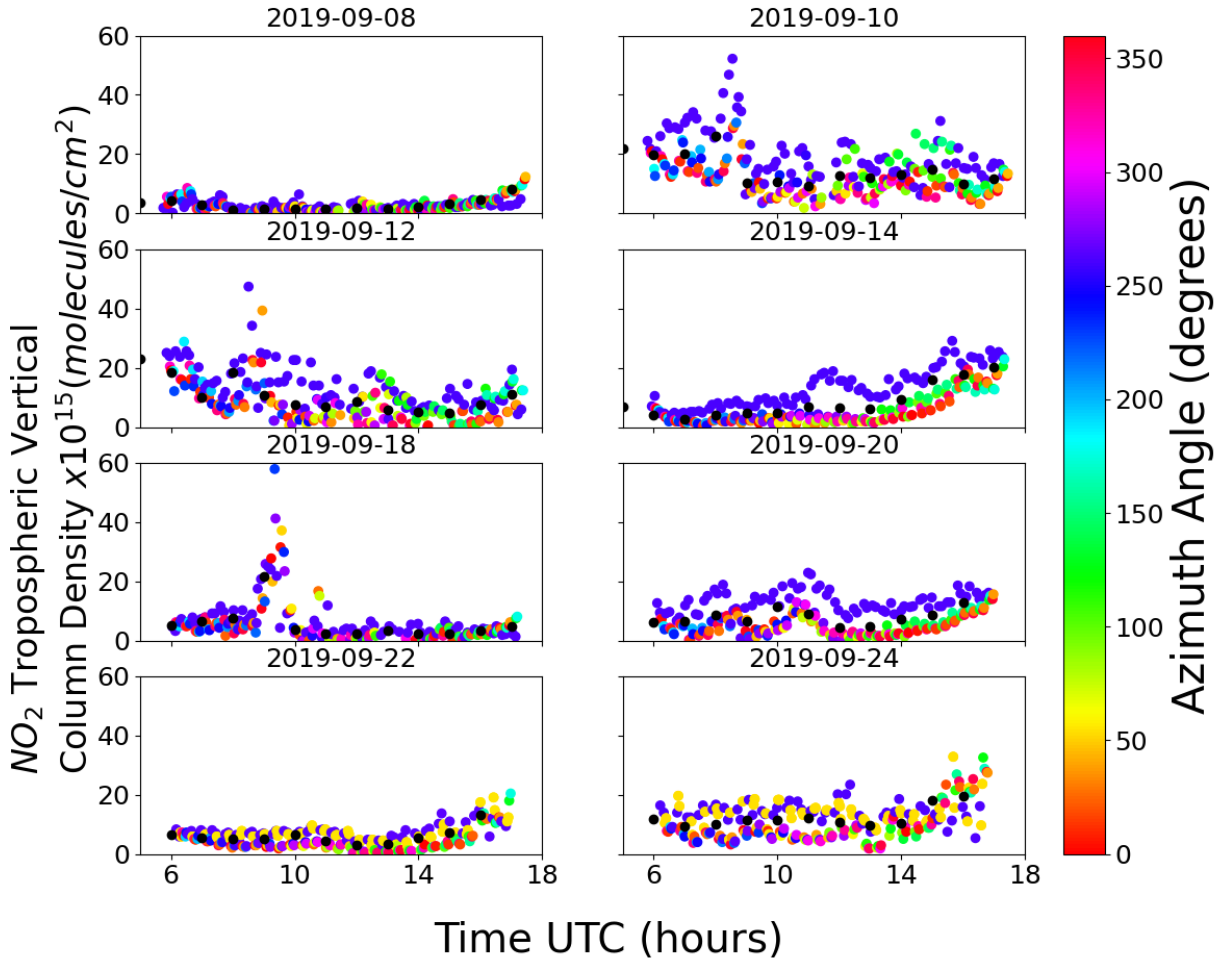

Figure 4.6: Time series NO_2 tropospheric vertical column densities for 8 days during the TROLIX'19 campaign in Rotterdam, NL. Black points correspond to the averaged MAX-DOAS values from the previous hour, and the color of each point is dependant on the azimuth viewing angle. Time is measured in hour in hours UTC

Figure 4.6 shows the time series of NO_2 tropospheric vertical column densities retrieved from MAX-DOAS measurements (Pandora 148) for 8 days during the TROLIX'19 campaign in Rotterdam, the Netherlands. The average VCD measured was approximately

$9 \times 10^{15}[\frac{molecules}{cm^2}]$ with a standard deviation of $8.5 \times 10^{15}[\frac{molecules}{cm^2}]$, which is both a higher level of pollution as well as a higher level of measurement variability than what was seen around Blacksburg, but also smaller than pollution levels seen by Wang et al. [49] at a rural site in Northern China. In addition to the higher levels of pollution, the spatial variability of NO_2 in Rotterdam is higher as well. This is especially clear on September 14th, when around noon, measurements made in the direction of the ship canal spiked, while measurements in the other directions remained low. If the ship canal measurements were used to validate TROPOMI then there would be an assumed much higher concentration of NO_2 at the measuring site than if any of the off-axis measurements were used.

4.3 Measurement Path Length and LOTOS-EUROS Simulated Profiles

Figure 4.7 shows the Vertical Column Densities LOTOS-EUROS simulated for September 12, 14, and 20 for 12pm In addition, the nearest TROPOMI pixel to the measuring site has been outlined in Black and the measuring site is represented by a pink dot. The exact location of the TROPOMI pixel relative to the measuring site shifts day to day. This occurs because the orbit of TROPOMI is not identical for each revolutionDepending on how the pixels align with the measuring site and the observation directions, measurements can be better used for validation for other satellite pixels that do not align with the measuring site. On 9/12/2019, for instance, measurements taken between 210° and 30° are not suitable for the pixel over the measuring site since the path lengths do not travel through the space observed by the pixel, instead the adjacent pixel would be validated by these measurements. The measurements to use for validation of each pixel also change depending on the day; this issue is mitigated by a general sampling strategy with many measurements made in an

orientation that is offset from the sun, so that a large enough set of measurements are made that measure a different air volumes from each other measurement, which can be used to validate the satellite pixel that is most spatially relevant to each measurement.

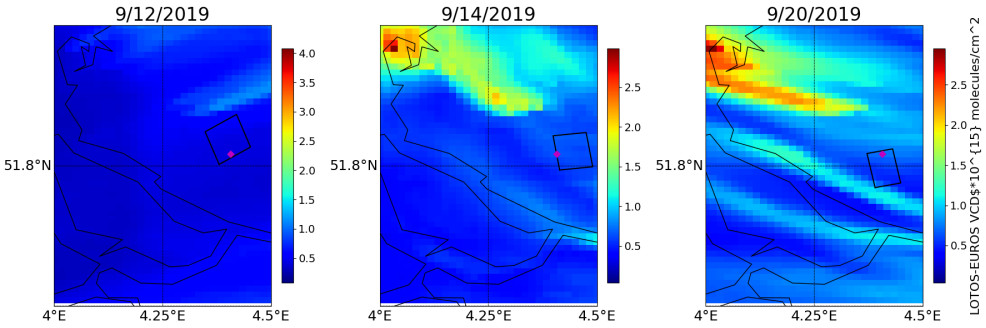

Figure 4.7: Map of the area surrounding the ground station in Rotterdam, the Netherlands (pink dot), and corresponding simulated LOTOS-EUROS Vertical Column Densities for September 12, 14, and 20. The nearest TROPOMI pixel on each day is outlined in black.

Figure 4.8 shows the simulated path lengths for the three days analyzed. Path lengths each day show a clear sensitivity to solar zenith angle in the morning and afternoon, which coincides with simulated path lengths in Blacksburg as well. The effective heights for measurements made at 75° zenith angles easily clear the Planetary Boundary Layer.Therefore, these simulated paths will fully travel through the tropospheric NO_2 profile, and can be used to evaluate measurement sensitivity to NO_2 profiles.

The simulated NO_2 profiles in Fig. 4.9 follow a similar pattern. Each day's simulated profiles are plotted alongside the estimated "TROPOMI" profile at the TROPOMI overpass time only. Morning profiles are very heterogeneous and vary greatly with viewing azimuth angle and are larger than the TROPOMI profile, however by the TROPOMI overpass time, the measured profiles much more homogeneous; however, the surface inhomogeneity is still clear, since most profiles are either larger or smaller that the TROPOMI profile. Rather than comparing individual profiles to the TROPOMI profile, the average of the set of profiles taken withing the hour of TROPOMI overpass would be a closer approximation, which

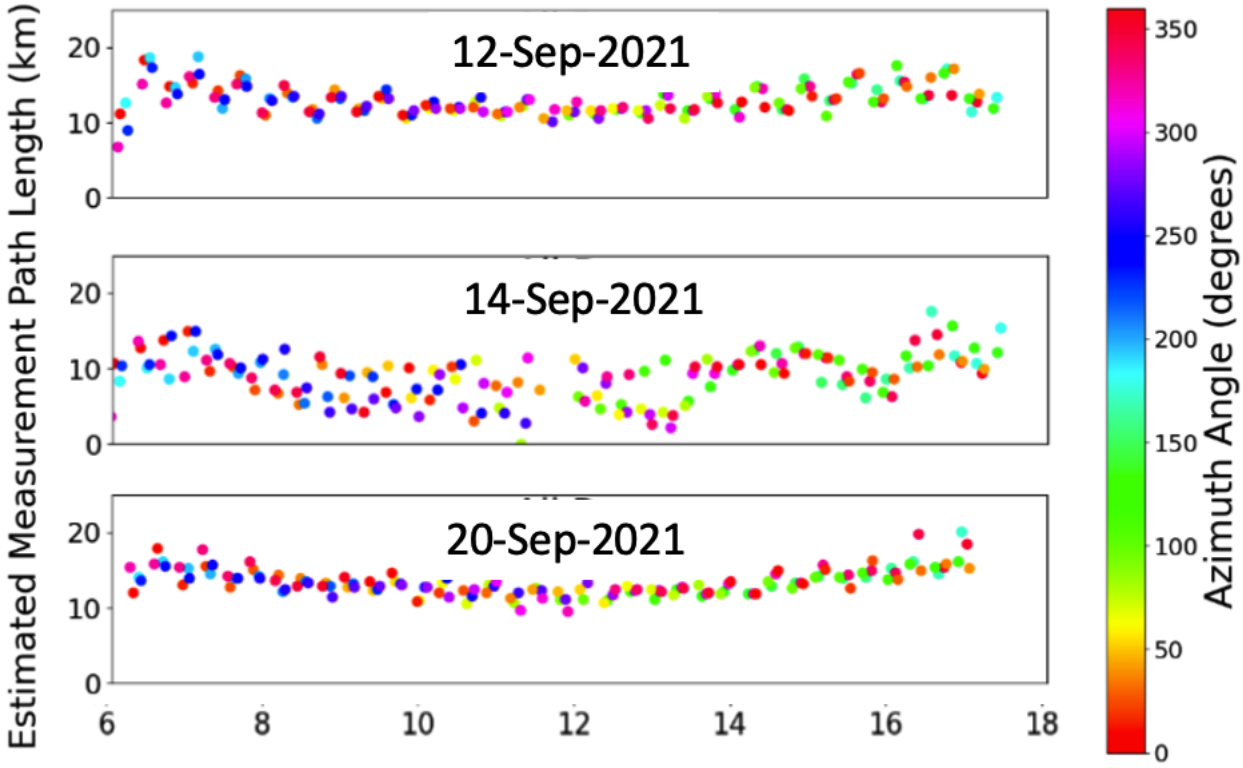

Figure 4.8: Time Series simulated path lengths based on measurements made during the TROLIX'19 field campaign. Each point is colored according to its azimuth viewing angle.

demonstrates the effectiveness of a spatially distributed measuring strategy. Since emissions, transport and photolysis change within the measurement volume based on the time of day, the satellite overpass time is also an important consideration to make when choosing a validation strategy. While TROPOMI only overpasses around 13:30 local time for all measured locations, TEMPO will be able to take measurements from sunrise to sunset at hourly intervals.

In addition, the measuring azimuth angles of the measurements to be averaged must relate to the area measured by the satellite pixel. This issue is illustrated best on September 20th. The profiles from measurements made that day, and in the hour around the TROPOMI overpass, were made in the northern direction, ranging from 300° to 100°. However, Figure

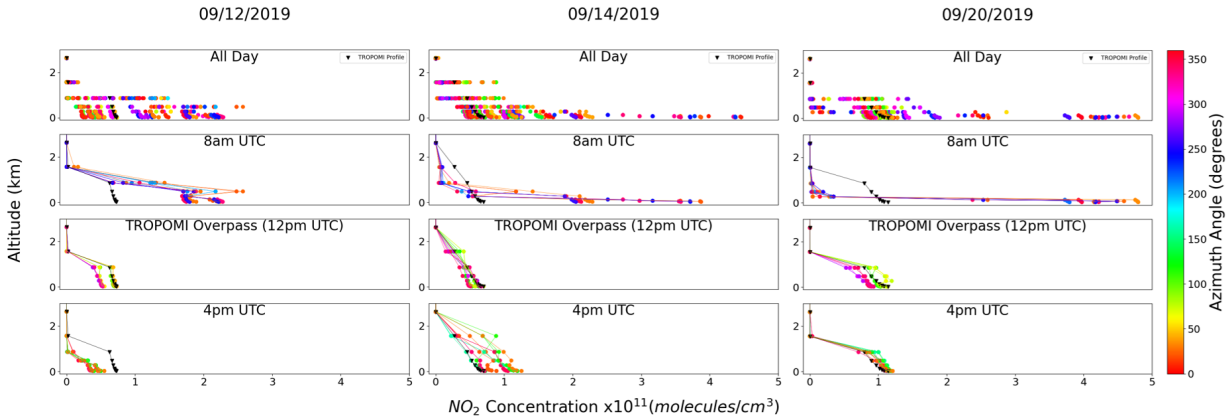

Figure 4.9: Simulated profiles based on measurements made during the TROLIX'19 field campaign on 9/12/2019,, 9/14/2019, and 9/20/2019 for the entire day, as well as specific hours: 8am, the relevant hour at which local TROPOMI measurements are taken, approximately 12pm and 4pm. Each point is colored according to its azimuth viewing angle.

4.7 shows that on September 20th, the measuring site is on the northern border of the relevant TROPOMI pixel. Measurement viewing angles between 250° and 70° would measure paths that mostly reside in a different pixel, and would be better used to validate that pixel instead. This issue highlights the need to have a sufficient number of measurements made at an even distribution of measuring azimuth angles, even if some of the measurements do not cover the pixel measuring area, there will always be enough to effectively measure the pixel measuring area.

One final consideration to make in regards to the profiles is the difference in profile shapes between the TROPOMI pixel and the simulated ground profiles. For instance the TROPOMI profile on September 12th is not only larger than the average ground measurement profile, the profile at the surface is slightly less sensitive than the ground measurements. This is also the case on September 14th, and is easier to see. The fact that the profiles seen by TROPOMI and round measurements are different demonstrates the fundamental problem with using individual measurements or a small number of averaged measurements to compare to satellite measurements. This lack of sensitivity to inhomogeneities of trace gas profiles by

space borne instruments means that measurements on the ground will need to have a similar lack of sensitivity, in order to measure a similar profile. Otherwise, since the measured profiles will be different, the retrieved column densities will be different. Since the point of validation is to ensure that measurements in space coincide with measurements on the ground, both measurements need to measure similar volumes of air, which should mean the profiles measured are the same. Therefore, since a lack of spatial averaging will lead to different trace gas profiles being measured on the ground and in space, a proper measuring strategy, that is able to measure azimuthaly similar volumes as the satellite to be validated, is the only effective way to validate satellite measurements.

Chapter 5

Conclusions

This paper demonstrates the effectiveness of spatially averaging MAX-DOAS measurements at regular azimuth angle intervals on an hourly basis to validate satellite based DOAS measurements. Off-Axis MAX-DOAS Measurements taken in Blacksburg, Virginia, between November 2021 and April 2022 with an evenly distributed set of measurements were averaged every hour and compared to Direct Sun measurements, also averaged every hour. Comparisons of the difference in average measurement from both measuring strategies, as well as the distribution standard deviations of hourly measurements suggests that the NO_2 distribution around Blacksburg is homogeneous, however the measuring strategy demonstrated a 30% reduction in average measurements compared to direct sun measurements.

In order to analyze the effects of hourly averaged sampling, the LOTOS-EUROS high resolution (1kmx1km) chemical transport model was used to simulate profiles and vertical column densities of real measurements taken in Rotterdam on September 12, 14, 20 during the TROLIX'19 Field Campaign. In order to estimate the length of the scattered light path, which is needed to determine the relevant model boxes that the measured light passed through, the differential slant column density of O_2O_2 measured on the ground is divided

by the concentration of O_2O_2 at the surface, which is calculated using meteorological data. Ground profiles vary greatly with both time and measuring viewing angle throughout the day, and comparisons to TROPOMI profiles, which have been simulated using model and real pixel geometries, show that the profiles observed are different from each other; however, the TROPOMI profile is approximately the average of all profiles simulated within an hour of the measuring time, which suggests that by spatially averaging measurements, an appropriate approximation of the profile seen from space can be made.

To summarize, in order to account for the lack of satellite sensitivity to horizontal inhomogeneity, a corresponding set of evenly distributed measurements in the azimuth direction can be averaged over a set time in order to decrease the azimuth sensitivity of ground measurements to better match satellite measurements, improving validation techniques. In order to ensure that the measurements coincide with what is seen by a satellite instrument, measurements taken within the hour of overpass should be averaged together in order to come to a measurement that covers an area that more closely resembles that which is seen by a satellite. In order to properly characterize, and remove, the sensitivity to horizontal inhomogeneities, the measurements averaged must be evenly distributed over the volume that is being measured by the satellite.

Chapter 6

Further Work

While this thesis demonstrates the viability of an hour based sampling strategy, the strategy needs to be field tested at an inhomogeneous location in order to truly determine its validity. Urban Locations, such as Greenbilt, Mayland where NASA's Goddard Spaceflight Center is located, is a sufficiently urban location to provide an inhomogeneous distribution of NO_2 that can be used to validate this measuring strategy. In addition, it is important to characterize just how many different viewing geometries are needed in order for the measuring strategy to be effective. An in depth look at the effect of various quantities of viewing geometries, distributed both in the azimuth and zenith directions, will not only prove the strategy's effectiveness, but also help to develop a plan of action for future satellite validation campaigns. However, in order to take enough measurements in a given hour, more instruments will need to be used. Rather than attempting to acquire more individual instruments to use, it would be better to instead develop a new instrument, that is able to take MAX-DOAS measurements in multiple zenith angles simultaneously at a given azimuth angle. The development and testing of this equipment would further aid in the development of the concepts in this thesis.

Bibliography

[1] K. F. Boersma, H. J. Eskes, and E. J. Brinksma. Error analysis for tropospheric NO2 retrieval from space. *Journal of Geophysical Research: Atmospheres*, 109(D4), 2004. ISSN 2156-2202. doi: 10.1029/2003JD003962. URL https://onlinelibrary.wiley.com/doi/abs/10.1029/2003JD003962. _eprint: https://onlinelibrary.wiley.com/doi/pdf/10.1029/2003JD003962.

[2] H. Bovensmann, J. P. Burrows, M. Buchwitz, J. Frerick, S. Noel, V. V. Rozanov, K. V. Chance, and A. P. H. Goede. SCIAMACHY: Mission Objectives and Measurement Modes. *JOURNAL OF THE ATMOSPHERIC SCIENCES*, 56(2):127–150, January 1999. doi: https://doi.org/10.1175/1520-0469(1999)056⟨0127:SMOAMM⟩2.0.CO;2.

[3] R. T. Brinkmann. Rotational Raman Scattering in Planetary Atmospheres. *The Astrophysical Journal*, 154:1087, December 1968. ISSN 0004-637X, 1538-4357. doi: 10.1086/149827. URL http://adsabs.harvard.edu/doi/10.1086/149827.

[4] Samuel M. Brohede, Craig S. Haley, Chris A. Mclinden, Christopher E. Sioris, Donal P. Murtagh, Svetlana V. Petelina, Edward J. Llewellyn, Ariane Bazureau, Florence Goutail, Cora E. Randall, Jerry D. Lumpe, Ghassan Taha, Larry W. Thomasson, and Larry L. Gordley. Validation of Odin/OSIRIS stratospheric NO_2 profiles. *Journal of Geophysical Research: Atmospheres*, 112:D07310, 2007. doi: 10.1029/2006JD007586.

URL https://hal.archives-ouvertes.fr/hal-00145004. Publisher: American Geophysical Union.

[5] E. J. Bucsela, N. A. Krotkov, E. A. Celarier, L. N. Lamsal, W. H. Swartz, P. K. Bhartia, K. F. Boersma, J. P. Veefkind, J. F. Gleason, and K. E. Pickering. A new stratospheric and tropospheric NO₂ retrieval algorithm for nadir-viewing satellite instruments: applications to OMI. *Atmospheric Measurement Techniques*, 6 (10):2607–2626, October 2013. ISSN 1867-8548. doi: 10.5194/amt-6-2607-2013. URL https://amt.copernicus.org/articles/6/2607/2013/.

[6] Alexander Cede. Manual for Blick Software Suite 1.8, April 2021. URL https://www.pandonia-global-network.org/home/documents/manuals/BlickSoftwareSuitev1-8.

[7] Ka Lok Chan, Matthias Wiegner, Jos van Geffen, Isabelle De Smedt, Carlos Alberti, Zhibin Cheng, Sheng Ye, and Mark Wenig. MAX-DOAS measurements of tropospheric NO₂ and HCHO in Munich and the comparison to OMI and TROPOMI satellite observations. *Atmospheric Measurement Techniques*, 13(8):4499–4520, August 2020. ISSN 1867-8548. doi: 10.5194/amt-13-4499-2020. URL https://amt.copernicus.org/articles/13/4499/2020/.

[8] Martine De Mazière, Anne M. Thompson, Michael J. Kurylo, Jeannette D. Wild, Germar Bernhard, Thomas Blumenstock, Geir O. Braathen, James W. Hannigan, Jean-Christopher Lambert, Thierry Leblanc, Thomas J. McGee, Gerald Nedoluha, Irina Petropavlovskikh, Gunther Seckmeyer, Paul C. Simon, Wolfgang Steinbrecht, and Susan E. Strahan. The Network for the Detection of Atmospheric Composition Change (NDACC): history, status and perspectives. *Atmospheric Chemistry and Physics*, 18

(7):4935–4964, April 2018. ISSN 1680-7324. doi: 10.5194/acp-18-4935-2018. URL https://acp.copernicus.org/articles/18/4935/2018/.

[9] Ermioni Dimitropoulou, François Hendrick, Gaia Pinardi, Martina M. Friedrich, Alexis Merlaud, Frederik Tack, Helene De Longueville, Caroline Fayt, Christian Hermans, Quentin Laffineur, Frans Fierens, and Michel Van Roozendael. Validation of TROPOMI tropospheric NO_2 columns using dual-scan multi-axis differential optical absorption spectroscopy (MAX-DOAS) measurements in Uccle, Brussels. *Atmospheric Measurement Techniques*, 13(10):5165–5191, October 2020. ISSN 1867-1381. doi: 10.5194/amt-13-5165-2020. URL https://amt.copernicus.org/articles/13/5165/2020/. Publisher: Copernicus GmbH.

[10] Theano Drosoglou, Alkiviadis F. Bais, Irene Zyrichidou, Natalia Kouremeti, Anastasia Poupkou, Natalia Liora, Christos Giannaros, Maria Elissavet Koukouli, Dimitris Balis, and Dimitrios Melas. Comparisons of ground-based tropospheric NO_2 MAX-DOAS measurements to satellite observations with the aid of an air quality model over the Thessaloniki area, Greece. *Atmospheric Chemistry and Physics*, 17(9):5829–5849, May 2017. ISSN 1680-7316. doi: 10.5194/acp-17-5829-2017. URL https://acp.copernicus.org/articles/17/5829/2017/. Publisher: Copernicus GmbH.

[11] U. Frieß, P. S. Monks, J. J. Remedios, A. Rozanov, R. Sinreich, T. Wagner, and U. Platt. MAX-DOAS O4 measurements: A new technique to derive information on atmospheric aerosols: 2. Modeling studies. *Journal of Geophysical Research: Atmospheres*, 111(D14), 2006. ISSN 2156-2202. doi: 10.1029/2005JD006618. URL https://onlinelibrary.wiley.com/doi/abs/10.1029/2005JD006618. _eprint: https://onlinelibrary.wiley.com/doi/pdf/10.1029/2005JD006618.

[12] Udo Frieß, Steffen Beirle, Leonardo Alvarado Bonilla, Tim Bösch, Martina M. Friedrich,

François Hendrick, Ankie Piters, Andreas Richter, Michel van Roozendael, Vladimir V. Rozanov, Elena Spinei, Jan-Lukas Tirpitz, Tim Vlemmix, Thomas Wagner, and Yang Wang. Intercomparison of MAX-DOAS vertical profile retrieval algorithms: studies using synthetic data. *Atmospheric Measurement Techniques*, 12(4):2155–2181, April 2019. ISSN 1867-8548. doi: 10.5194/amt-12-2155-2019. URL https://amt.copernicus.org/articles/12/2155/2019/.

[13] Jeffrey A. Geddes, Randall V. Martin, Eric J. Bucsela, Chris A. McLinden, and Daniel J. M. Cunningham. Stratosphere–troposphere separation of nitrogen dioxide columns from the TEMPO geostationary satellite instrument. *Atmospheric Measurement Techniques*, 11(11):6271–6287, November 2018. ISSN 1867-8548. doi: 10.5194/amt-11-6271-2018. URL https://amt.copernicus.org/articles/11/6271/2018/.

[14] Daniel L. Goldberg, Susan C. Anenberg, Gaige Hunter Kerr, Arash Mohegh, Zifeng Lu, and David G. Streets. TROPOMI NO2 in the United States: A Detailed Look at the Annual Averages, Weekly Cycles, Effects of Temperature, and Correlation With Surface NO2 Concentrations. *Earth's Future*, 9(4):e2020EF001665, 2021. ISSN 2328-4277. doi: 10.1029/2020EF001665. URL https://onlinelibrary.wiley.com/doi/abs/10.1029/2020EF001665. _eprint: https://onlinelibrary.wiley.com/doi/pdf/10.1029/2020EF001665.

[15] J. F. Grainger and J. Ring. Anomalous Fraunhofer Line Profiles. *Nature*, 193(4817): 762–762, February 1962. ISSN 0028-0836, 1476-4687. doi: 10.1038/193762a0. URL https://www.nature.com/articles/193762a0.

[16] Jörg Heland, Hans Schlager, Andreas Richter, and John P. Burrows. First comparison of tropospheric NO2 column densities retrieved from GOME measurements and in situ aircraft profile measurements. *Geophysical Research Let-*

ters, 29(20):44–1–44–4, 2002. ISSN 1944-8007. doi: 10.1029/2002GL015528. URL https://onlinelibrary.wiley.com/doi/abs/10.1029/2002GL015528. _eprint: https://onlinelibrary.wiley.com/doi/pdf/10.1029/2002GL015528.

[17] Thomas W. Hesterberg, William B. Bunn, Roger O. McClellan, Ali K. Hamade, Christopher M. Long, and Peter A. Valberg. Critical review of the human data on short-term nitrogen dioxide (NO $_2$) exposures: Evidence for NO $_2$ no-effect levels. *Critical Reviews in Toxicology*, 39(9):743–781, October 2009. ISSN 1040-8444, 1547-6898. doi: 10.3109/10408440903294945. URL http://www.tandfonline.com/doi/full/10.3109/10408440903294945.

[18] G. Hönninger, C. von Friedeburg, and U. Platt. Multi axis differential optical absorption spectroscopy (MAX-DOAS). *Atmospheric Chemistry and Physics*, 4(1):231–254, February 2004. ISSN 1680-7316. doi: 10.5194/acp-4-231-2004. URL https://acp.copernicus.org/articles/4/231/2004/. Publisher: Copernicus GmbH.

[19] Iolanda Ialongo, Henrik Virta, Henk Eskes, Jari Hovila, and John Douros. Comparison of TROPOMI/Sentinel-5 Precursor NO_2 observations with ground-based measurements in Helsinki. *Atmospheric Measurement Techniques*, 13(1):205–218, January 2020. ISSN 1867-1381. doi: 10.5194/amt-13-205-2020. URL https://amt.copernicus.org/articles/13/205/2020/. Publisher: Copernicus GmbH.

[20] D.V. Ionov, Valery P. Sinyakov, and V.K. Semenov. Validation of GOME (ERS-2) NO2 vertical column data with ground-based measurements at ISSyk-Kul (Kyrgyzstan). *Advances in Space Research*, 37:2254–2260, November 2005. doi: doi:10.1016/j.asr.2005.11.011.

[21] Karin Kreher, Michel Van Roozendael, Francois Hendrick, Arnoud Apituley, Ermioni Dimitropoulou, Udo Frieß, Andreas Richter, Thomas Wagner, Johannes Lampel, Nader

Abuhassan, Li Ang, Monica Anguas, Alkis Bais, Nuria Benavent, Tim Bösch, Kristof Bognar, Alexander Borovski, Ilya Bruchkouski, Alexander Cede, Ka Lok Chan, Sebastian Donner, Theano Drosoglou, Caroline Fayt, Henning Finkenzeller, David Garcia-Nieto, Clio Gielen, Laura Gómez-Martín, Nan Hao, Bas Henzing, Jay R. Herman, Christian Hermans, Syedul Hoque, Hitoshi Irie, Junli Jin, Paul Johnston, Junaid Khayyam Butt, Fahim Khokhar, Theodore K. Koenig, Jonas Kuhn, Vinod Kumar, Cheng Liu, Jianzhong Ma, Alexis Merlaud, Abhishek K. Mishra, Moritz Müller, Monica Navarro-Comas, Mareike Ostendorf, Andrea Pazmino, Enno Peters, Gaia Pinardi, Manuel Pinharanda, Ankie Piters, Ulrich Platt, Oleg Postylyakov, Cristina Prados-Roman, Olga Puentedura, Richard Querel, Alfonso Saiz-Lopez, Anja Schönhardt, Stefan F. Schreier, André Seyler, Vinayak Sinha, Elena Spinei, Kimberly Strong, Frederik Tack, Xin Tian, Martin Tiefengraber, Jan-Lukas Tirpitz, Jeroen van Gent, Rainer Volkamer, Mihalis Vrekoussis, Shanshan Wang, Zhuoru Wang, Mark Wenig, Folkard Wittrock, Pinhua H. Xie, Jin Xu, Margarita Yela, Chengxin Zhang, and Xiaoyi Zhao. Intercomparison of NO₂, O₄, O₃ and HCHO slant column measurements by MAX-DOAS and zenith-sky UV–visible spectrometers during CINDI-2. *Atmospheric Measurement Techniques*, 13(5):2169–2208, May 2020. ISSN 1867-8548. doi: 10.5194/amt-13-2169-2020. URL https://amt.copernicus.org/articles/13/2169/2020/.

[22] Pieternel F. Levelt, Joanna Joiner, Johanna Tamminen, J. Pepijn Veefkind, Pawan K. Bhartia, Deborah C. Stein Zweers, Bryan N. Duncan, David G. Streets, Henk Eskes, Ronald van der A, Chris McLinden, Vitali Fioletov, Simon Carn, Jos de Laat, Matthew DeLand, Sergey Marchenko, Richard McPeters, Jerald Ziemke, Dejian Fu, Xiong Liu, Kenneth Pickering, Arnoud Apituley, Gonzalo González Abad, Antti Arola, Folkert Boersma, Christopher Chan Miller, Kelly Chance, Martin de Graaf, Janne Hakkarainen,

Seppo Hassinen, Iolanda Ialongo, Quintus Kleipool, Nickolay Krotkov, Can Li, Lok Lamsal, Paul Newman, Caroline Nowlan, Raid Suleiman, Lieuwe Gijsbert Tilstra, Omar Torres, Huiqun Wang, and Krzysztof Wargan. The Ozone Monitoring Instrument: overview of 14 years in space. *Atmospheric Chemistry and Physics*, 18(8):5699–5745, April 2018. ISSN 1680-7324. doi: 10.5194/acp-18-5699-2018. URL https://acp.copernicus.org/articles/18/5699/2018/.

[23] X. Li, T. Brauers, A. Hofzumahaus, K. Lu, Y. P. Li, M. Shao, T. Wagner, and A. Wahner. MAX-DOAS measurements of NO_2, HCHO and CHOCHO at a rural site in Southern China. *Atmospheric Chemistry and Physics*, 13(4):2133–2151, February 2013. ISSN 1680-7316. doi: 10.5194/acp-13-2133-2013. URL https://acp.copernicus.org/articles/13/2133/2013/. Publisher: Copernicus GmbH.

[24] D. G. Loyola, M. E. Koukouli, P. Valks, D. S. Balis, N. Hao, M. Van Roozendael, R. J. D. Spurr, W. Zimmer, S. Kiemle, C. Lerot, and J.-C. Lambert. The GOME-2 total column ozone product: Retrieval algorithm and ground-based validation. *Journal of Geophysical Research: Atmospheres*, 116(D7), 2011. ISSN 2156-2202. doi: 10.1029/2010JD014675. URL https://onlinelibrary.wiley.com/doi/abs/10.1029/2010JD014675. _eprint: https://onlinelibrary.wiley.com/doi/pdf/10.1029/2010JD014675.

[25] Astrid M. M. Manders, Peter J. H. Builtjes, Lyana Curier, Hugo A. C. Denier van der Gon, Carlijn Hendriks, Sander Jonkers, Richard Kranenburg, Jeroen J. P. Kuenen, Arjo J. Segers, Renske M. A. Timmermans, Antoon J. H. Visschedijk, Roy J. Wichink Kruit, W. Addo J. van Pul, Ferd J. Sauter, Eric van der Swaluw, Daan P. J. Swart, John Douros, Henk Eskes, Erik van Meijgaard, Bert van Ulft, Peter van Velthoven, Sabine Banzhaf, Andrea C. Mues, Rainer Stern, Guangliang Fu, Sha Lu, Arnold Heemink, Nils van Velzen, and Martijn Schaap. Curriculum vitae of the LOTOS–EUROS (v2.0) chemistry transport model. *Geoscientific Model Development*, 10

(11):4145–4173, November 2017. ISSN 1991-9603. doi: 10.5194/gmd-10-4145-2017. URL https://gmd.copernicus.org/articles/10/4145/2017/.

[26] Randall V. Martin. An improved retrieval of tropospheric nitrogen dioxide from GOME. *Journal of Geophysical Research*, 107(D20):4437, 2002. ISSN 0148-0227. doi: 10.1029/2001JD001027. URL http://doi.wiley.com/10.1029/2001JD001027.

[27] Richard Meller and Geert K. Moortgat. Temperature dependence of the absorption cross sections of formaldehyde between 223 and 323 K in the wavelength range 225–375 nm. *Journal of Geophysical Research: Atmospheres*, 105(D6):7089–7101, 2000. ISSN 2156-2202. doi: 10.1029/1999JD901074. URL https://onlinelibrary.wiley.com/doi/abs/10.1029/1999JD901074. _eprint: https://onlinelibrary.wiley.com/doi/pdf/10.1029/1999JD901074.

[28] Rosemary Munro, Rüdiger Lang, Dieter Klaes, Gabriele Poli, Christian Retscher, Rasmus Lindstrot, Roger Huckle, Antoine Lacan, Michael Grzegorski, Andriy Holdak, Alexander Kokhanovsky, Jakob Livschitz, and Michael Eisinger. The GOME-2 instrument on the Metop series of satellites: instrument design, calibration, and level 1 data processing – an overview. *Atmospheric Measurement Techniques*, 9(3):1279–1301, March 2016. ISSN 1867-8548. doi: 10.5194/amt-9-1279-2016. URL https://amt.copernicus.org/articles/9/1279/2016/.

[29] Gaia Pinardi, Michel Van Roozendael, François Hendrick, Nicolas Theys, Nader Abuhassan, Alkiviadis Bais, Folkert Boersma, Alexander Cede, Jihyo Chong, Sebastian Donner, Theano Drosoglou, Anatoly Dzhola, Henk Eskes, Udo Frieß, José Granville, Jay R. Herman, Robert Holla, Jari Hovila, Hitoshi Irie, Yugo Kanaya, Dimitris Karagkiozidis, Natalia Kouremeti, Jean-Christopher Lambert, Jianzhong Ma, Enno Peters, Ankie Piters, Oleg Postylyakov, Andreas Richter, Julia Remmers, Hisahiro

Takashima, Martin Tiefengraber, Pieter Valks, Tim Vlemmix, Thomas Wagner, and Folkard Wittrock. Validation of tropospheric NO₂ column measurements of GOME-2A and OMI using MAX-DOAS and direct sun network observations. *Atmospheric Measurement Techniques*, 13(11):6141–6174, November 2020. ISSN 1867-8548. doi: 10.5194/amt-13-6141-2020. URL https://amt.copernicus.org/articles/13/6141/2020/.

[30] A J M Piters and K Bramstedt. Overview of SCIAMACHY validation: 2002–2004. *Atmos. Chem. Phys.*, page 22, 2006.

[31] Ulrich Platt and Jochen Stutz. *Differential Optical Absorption Spectroscopy*. Springer-Verlag Berlin Heidelberg, 1st edition, 2008. ISBN 978-3-540-75776-4.

[32] J P Pommereau and J Piquard. Ozone, nitrogen dioxide and aerosol vertical distribution by UV-visible solar occultation from balloons. *Geophysical Research Letters (American Geophysical Union*, 21:13, June 1994. doi: https://doi.org/10.1029/94GL00389.

[33] Elmer Robinson and Robert C. Robbins. Gaseous Nitrogen Compound Pollutants from Urban and Natural Sources. *Journal of the Air Pollution Control Association*, 20(5): 303–306, May 1970. ISSN 0002-2470. doi: 10.1080/00022470.1970.10469405. URL https://www.tandfonline.com/doi/full/10.1080/00022470.1970.10469405.

[34] Robert A. Rohde and Richard A. Muller. Air Pollution in China: Mapping of Concentrations and Sources. *PLOS ONE*, 10(8):e0135749, August 2015. ISSN 1932-6203. doi: 10.1371/journal.pone.0135749. URL https://dx.plos.org/10.1371/journal.pone.0135749.

[35] L. S. Rothman, I. E. Gordon, Y. Babikov, A. Barbe, D. Chris Benner, P. F. Bernath, M. Birk, L. Bizzocchi, V. Boudon, L. R. Brown, A. Campargue, K. Chance, E. A. Cohen,

L. H. Coudert, V. M. Devi, B. J. Drouin, A. Fayt, J.-M. Flaud, R. R. Gamache, J. J. Harrison, J.-M. Hartmann, C. Hill, J. T. Hodges, D. Jacquemart, A. Jolly, J. Lamouroux, R. J. Le Roy, G. Li, D. A. Long, O. M. Lyulin, C. J. Mackie, S. T. Massie, S. Mikhailenko, H. S. P. Müller, O. V. Naumenko, A. V. Nikitin, J. Orphal, V. Perevalov, A. Perrin, E. R. Polovtseva, C. Richard, M. A. H. Smith, E. Starikova, K. Sung, S. Tashkun, J. Tennyson, G. C. Toon, Vl G. Tyuterev, and G. Wagner. The HITRAN2012 molecular spectroscopic database. *Journal of Quantitative Spectroscopy and Radiative Transfer*, 130:4–50, 2013. ISSN 0022-4073. doi: https://doi.org/10.1016/j.jqsrt.2013.07.002. URL https://www.sciencedirect.com/science/article/pii/S0022407313002859.

[36] D. Schaub, D. Brunner, K. F. Boersma, J. Keller, D. Folini, B. Buchmann, H. Berresheim, and J. Staehelin. SCIAMACHY tropospheric NO₂ over Switzerland: estimates of NO_x lifetimes and impact of the complex Alpine topography on the retrieval. *Atmospheric Chemistry and Physics*, 7(23):5971–5987, December 2007. ISSN 1680-7324. doi: 10.5194/acp-7-5971-2007. URL https://acp.copernicus.org/articles/7/5971/2007/.

[37] Josef Schreder. Instruction Manual: Find Clouds Software, 2017.

[38] A. Serdyuchenko, V. Gorshelev, M. Weber, W. Chehade, and J. P. Burrows. High spectral resolution ozone absorption cross-sections – Part 2: Temperature dependence. *Atmospheric Measurement Techniques*, 7(2):625–636, February 2014. ISSN 1867-8548. doi: 10.5194/amt-7-625-2014. URL https://amt.copernicus.org/articles/7/625/2014/.

[39] Jonathan M Snowden, Kathleen M Mortimer, Mi-Suk Kang Dufour, and Ira B Tager. Population intervention models to estimate ambient NO2 health effects in children with

asthma. *Journal of Exposure Science & Environmental Epidemiology*, 25(6):567–573, November 2015. ISSN 1559-0631, 1559-064X. doi: 10.1038/jes.2014.60. URL https://www.nature.com/articles/jes201460.

[40] E. Spinei, A. Cede, W. H. Swartz, J. Herman, and G. H. Mount. The use of NO₂ absorption cross section temperature sensitivity to derive NO₂ profile temperature and stratospheric–tropospheric column partitioning from visible direct-sun DOAS measurements. *Atmospheric Measurement Techniques*, 7(12):4299–4316, December 2014. ISSN 1867-8548. doi: 10.5194/amt-7-4299-2014. URL https://amt.copernicus.org/articles/7/4299/2014/.

[41] Elena Spinei, Andrew Whitehill, Alan Fried, Martin Tiefengraber, Travis N. Knepp, Scott Herndon, Jay R. Herman, Moritz Müller, Nader Abuhassan, Alexander Cede, Dirk Richter, James Walega, James Crawford, James Szykman, Lukas Valin, David J. Williams, Russell Long, Robert J. Swap, Youngjae Lee, Nabil Nowak, and Brett Poche. The first evaluation of formaldehyde column observations by improved Pandora spectrometers during the KORUS-AQ field study. *Atmospheric Measurement Techniques*, 11(9):4943–4961, August 2018. ISSN 1867-8548. doi: 10.5194/amt-11-4943-2018. URL https://amt.copernicus.org/articles/11/4943/2018/.

[42] Ryan Thalman and Rainer Volkamer. Temperature dependent absorption cross-sections of o 2–o 2 colli sion pairs between 340 and 630 nm and at atmospherically relevant pressure. *Physical Chemistry Chemical Physics*, (37), 2013. doi: 10.1039/c3cp50968k.

[43] Jan-Lukas Tirpitz, Udo Frieß, François Hendrick, Carlos Alberti, Marc Allaart, Arnoud Apituley, Alkis Bais, Steffen Beirle, Stijn Berkhout, Kristof Bognar, Tim Bösch, Ilya Bruchkouski, Alexander Cede, Ka Lok Chan, Mirjam den Hoed, Sebastian Donner, Theano Drosoglou, Caroline Fayt, Martina M. Friedrich, Arnoud Frumau, Lou Gast,

Clio Gielen, Laura Gomez-Martín, Nan Hao, Arjan Hensen, Bas Henzing, Christian Hermans, Junli Jin, Karin Kreher, Jonas Kuhn, Johannes Lampel, Ang Li, Cheng Liu, Haoran Liu, Jianzhong Ma, Alexis Merlaud, Enno Peters, Gaia Pinardi, Ankie Piters, Ulrich Platt, Olga Puentedura, Andreas Richter, Stefan Schmitt, Elena Spinei, Deborah Stein Zweers, Kimberly Strong, Daan Swart, Frederik Tack, Martin Tiefengraber, René van der Hoff, Michel van Roozendael, Tim Vlemmix, Jan Vonk, Thomas Wagner, Yang Wang, Zhuoru Wang, Mark Wenig, Matthias Wiegner, Folkard Wittrock, Pinhua Xie, Chengzhi Xing, Jin Xu, Margarita Yela, Chengxin Zhang, and Xiaoyi Zhao. Intercomparison of MAX-DOAS vertical profile retrieval algorithms: studies on field data from the CINDI-2 campaign. *Atmospheric Measurement Techniques*, 14(1):1–35, January 2021. ISSN 1867-8548. doi: 10.5194/amt-14-1-2021. URL https://amt.copernicus.org/articles/14/1/2021/.

[44] OAR US EPA. Nitrogen Dioxide (NO2) Pollution, March 2016. URL https://www.epa.gov/no2-pollution.

[45] J. H. G. M. van Geffen, K. F. Boersma, M. Van Roozendael, F. Hendrick, E. Mahieu, I. De Smedt, M. Sneep, and J. P. Veefkind. Improved spectral fitting of nitrogen dioxide from OMI in the 405–465 nm window. *Atmospheric Measurement Techniques*, 8(4): 1685–1699, April 2015. ISSN 1867-8548. doi: 10.5194/amt-8-1685-2015. URL https://amt.copernicus.org/articles/8/1685/2015/.

[46] A. C. Vandaele, C. Hermans, P. C. Simon, M. Carleer, R. Colin, S. Fally, M. F. Mérienne, A. Jenouvrier, and B. Coquart. Measurements of the NO2 absorption cross-section from 42 000 cm1 to 10 000 cm1 (238–1000 nm) at 220 K and 294 K. *Journal of Quantitative Spectroscopy and Radiative Transfer*, 59(3):171–184, 1998. ISSN 0022-4073. doi: https://doi.org/10.1016/S0022-4073(97)00168-4. URL https://www.sciencedirect.com/science/article/pii/S0022407397001684.

[47] Tijl Verhoelst, Steven Compernolle, Gaia Pinardi, Jean-Christopher Lambert, Henk J. Eskes, Kai-Uwe Eichmann, Ann Mari Fjæraa, José Granville, Sander Niemeijer, Alexander Cede, Martin Tiefengraber, François Hendrick, Andrea Pazmiño, Alkiviadis Bais, Ariane Bazureau, K. Folkert Boersma, Kristof Bognar, Angelika Dehn, Sebastian Donner, Aleksandr Elokhov, Manuel Gebetsberger, Florence Goutail, Michel Grutter de la Mora, Aleksandr Gruzdev, Myrto Gratsea, Georg H. Hansen, Hitoshi Irie, Nis Jepsen, Yugo Kanaya, Dimitris Karagkiozidis, Rigel Kivi, Karin Kreher, Pieternel F. Levelt, Cheng Liu, Moritz Müller, Monica Navarro Comas, Ankie J. M. Piters, Jean-Pierre Pommereau, Thierry Portafaix, Cristina Prados-Roman, Olga Puentedura, Richard Querel, Julia Remmers, Andreas Richter, John Rimmer, Claudia Rivera Cárdenas, Lidia Saavedra de Miguel, Valery P. Sinyakov, Wolfgang Stremme, Kimberly Strong, Michel Van Roozendael, J. Pepijn Veefkind, Thomas Wagner, Folkard Wittrock, Margarita Yela González, and Claus Zehner. Ground-based validation of the Copernicus Sentinel-5P TROPOMI NO_2 measurements with the NDACC ZSL-DOAS, MAX-DOAS and Pandonia global networks. *Atmospheric Measurement Techniques*, 14(1): 481–510, January 2021. ISSN 1867-1381. doi: 10.5194/amt-14-481-2021. URL https://amt.copernicus.org/articles/14/481/2021/. Publisher: Copernicus GmbH.

[48] Y. Wang, A. Li, P. H. Xie, T. Wagner, H. Chen, W. Q. Liu, and J. G. Liu. A rapid method to derive horizontal distributions of trace gases and aerosols near the surface using multi-axis differential optical absorption spectroscopy. *Atmospheric Measurement Techniques*, 7(6):1663–1680, June 2014. ISSN 1867-8548. doi: 10.5194/amt-7-1663-2014. URL https://amt.copernicus.org/articles/7/1663/2014/.

[49] Yang Wang, Steffen Dörner, Sebastian Donner, Sebastian Böhnke, Isabelle De Smedt, Russell R. Dickerson, Zipeng Dong, Hao He, Zhanqing Li, Zhengqiang Li, Donghui Li, Dong Liu, Xinrong Ren, Nicolas Theys, Yuying Wang, Yang Wang, Zhenzhu Wang, Hua

Xu, Jiwei Xu, and Thomas Wagner. Vertical profiles of NO₂, SO₂, HONO, HCHO, CHOCHO and aerosols derived from MAX-DOAS measurements at a rural site in the central western North China Plain and their relation to emission sources and effects of regional transport. *Atmospheric Chemistry and Physics*, 19(8):5417–5449, April 2019. ISSN 1680-7324. doi: 10.5194/acp-19-5417-2019. URL https://acp.copernicus.org/articles/19/5417/2019/.

[50] Yehui Zhang, Dian Seidel, and Shaodong Zhang. Trends in Planetary Boundary Layer Height over Europe. *Journal of Climate*, 26(24):10071–10076, February 2013. doi: 10.1175/JCLI-D-13-00108.1.

[51] Xiaoyi Zhao, Debora Griffin, Vitali Fioletov, Chris McLinden, Alexander Cede, Martin Tiefengraber, Moritz Müller, Kristof Bognar, Kimberly Strong, Folkert Boersma, Henk Eskes, Jonathan Davies, Akira Ogyu, and Sum Chi Lee. Assessment of the quality of TROPOMI high-spatial-resolution NO_2 data products in the Greater Toronto Area. *Atmospheric Measurement Techniques*, 13(4):2131–2159, April 2020. ISSN 1867-1381. doi: 10.5194/amt-13-2131-2020. URL https://amt.copernicus.org/articles/13/2131/2020/. Publisher: Copernicus GmbH.

[52] P. Zoogman, X. Liu, R.M. Suleiman, W.F. Pennington, D.E. Flittner, J.A. Al-Saadi, B.B. Hilton, D.K. Nicks, M.J. Newchurch, J.L. Carr, S.J. Janz, M.R. Andraschko, A. Arola, B.D. Baker, B.P. Canova, C. Chan Miller, R.C. Cohen, J.E. Davis, M.E. Dussault, D.P. Edwards, J. Fishman, A. Ghulam, G. González Abad, M. Grutter, J.R. Herman, J. Houck, D.J. Jacob, J. Joiner, B.J. Kerridge, J. Kim, N.A. Krotkov, L. Lamsal, C. Li, A. Lindfors, R.V. Martin, C.T. McElroy, C. McLinden, V. Natraj, D.O. Neil, C.R. Nowlan, E.J. O'Sullivan, P.I. Palmer, R.B. Pierce, M.R. Pippin, A. Saiz-Lopez, R.J.D. Spurr, J.J. Szykman, O. Torres, J.P. Veefkind, B. Veihelmann, H. Wang, J. Wang, and K. Chance. Tropospheric Emissions: Monitor-

ing of Pollution (TEMPO). *Journal of quantitative spectroscopy & radiative transfer*, 186:17–39, January 2017. ISSN 0022-4073. doi: 10.1016/j.jqsrt.2016.05.008. URL https://www.ncbi.nlm.nih.gov/pmc/articles/PMC7430511/.